Clim. Past, 20, 547–571, 2024
https://doi.org/10.5194/cp-20-547-2024

Climate of the Past
Open Access
EGU

Sea-level and monsoonal control on the Maldives carbonate platform (Indian Ocean) over the last 1.3 million years

Montserrat Alonso-Garcia[1,2], Jesus Reolid[3], Francisco J. Jimenez-Espejo[4], Or M. Bialik[5,6], Carlos A. Alvarez Zarikian[7], Juan Carlos Laya[8], Igor Carrasquiera[9], Luigi Jovane[9], John J. G. Reijmer[10], Gregor P. Eberli[11], and Christian Betzler[12]

[1]Dpto. Geologia, Universidad de Salamanca, Pza de los caídos s/n, 37008 Salamanca, Spain
[2]Centro de Ciencias do Mar (CCMAR), Universidade do Algarve, Campus de Gambelas, 8005-139 Faro, Portugal
[3]Departamento de Estratigrafía y Paleontología, Facultad de Ciencias, Universidad de Granada, Avenida de la Fuente Nueva S/N, 18071 Granada, Spain
[4]Instituto Andaluz de Ciencias de la Tierra (CSIC-UGR), Avda. de las Palmeras 4, 18100 Armilla, Spain
[5]Institute of Geology and Palaeontology, University of Münster, Münster, Germany
[6]Dr. Moses Strauss Department of Marine Geosciences, Charney School of Marine Sciences, University of Haifa, 3498838 Haifa, Israel
[7]International Ocean Discovery Program, Texas A&M University, College Station, Texas, 77845, USA
[8]Department of Geology and Geophysics, Texas A&M University, College Station, Texas, 77843, USA
[9]Instituto Oceanográfico, Universidade de São Paulo, Praça do Oceanográfico, 191, São Paulo, SP, 05508-120, Brazil
[10]Faculty of Science, Vrije Universiteit Amsterdam, 1081 HV Amsterdam, the Netherlands
[11]Center for Carbonate Research, Department of Marine Geosciences, Rosenstiel School of Marine and Atmospheric Science, University of Miami, 4600 Rickenbacker Causeway, Miami, FL 33149, USA
[12]Institute of Geology, CEN, University of Hamburg, Bundesstraße 55, 20146 Hamburg, Germany

Correspondence: Montserrat Alonso-Garcia (montseag@usal.es) and Jesus Reolid (jreolid@ugr.es)

Received: 28 August 2023 – Discussion started: 5 September 2023
Accepted: 22 January 2024 – Published: 18 March 2024

Abstract. The Maldives Archipelago (Indian Ocean), composed of two rows of atolls that enclose an inner sea, offers an excellent study site to explore the forcings of carbonate production at platforms. Glacial–interglacial sea-level changes have been claimed to be the main factor controlling the carbonate platform factories; however, climatic factors may also have an impact. In this work we used geochemical compositional records, obtained by X-ray fluorescence (XRF) core-scanning from the International Ocean Discovery Program (IODP) Site U1467 in the Maldives Inner Sea, to analyze the orbitally driven fluctuations on the carbonate production and export from the neritic environment into the Maldives Inner Sea over the last 1.3 million years.

High Sr aragonite-rich carbonates (HSAC) from neritic settings were deposited in the Maldives Inner Sea during sea-level highstand intervals, increasing the Sr/Ca values. In contrast, low Sr/Ca values are observed coincident with sea-level lowstand periods, suggesting that large areas of the atolls were exposed or unable to grow, and therefore, there was a demise in the carbonate production and sediment export to the Maldives Inner Sea. However, comparison of the Sr/Ca values and the sea-level reconstructions for different interglacial periods before and after the mid-Brunhes event (MBE, ∼ 430 ka) indicates that sea level is not the only factor controlling the production of HSAC during sea-level highstands. The study of monsoon and primary productivity proxies (Fe-normalized, Fe/K, and Br-normalized records) from the same site suggests that the intensity of the summer monsoon and the Indian Ocean dipole probably modulated the carbonate production at the atolls. Moreover, Marine Isotope Stage 11 stands out as a period with high sea level and extraordinary carbonate production in the Maldives platform. This outstanding carbonate production in the Maldives atolls (and in other low-latitude carbonate platforms) proba-

bly contributed to the mid-Brunhes dissolution event through a strong shelf-to-basin fractionation of carbonate deposition.

1 Introduction

During the Quaternary, the Earth's climate oscillated between cold and warm periods due to variations in the planet's orbital parameters that drove the waxing and waning of the ice sheets and the establishment of glacial–interglacial cycles. During the Early Pleistocene these cycles were paced by obliquity (~ 41 kyr duration), whereas during the Mid-Pleistocene transition (MPT) the 100 kyr cyclicity emerged, characterizing the Late Pleistocene glacial–interglacial oscillations (Imbrie et al., 1993; Raymo, 1994; Raymo et al., 2006). The drivers behind this switch in the glacial–interglacial cyclicity are still debated since there was no change in the astronomical forcing and the effect of eccentricity as insolation forcing is too low to explain the 100 kyr cyclicity (Berger et al., 2005; Lisiecki, 2010). Therefore, the emergence of this climatic cyclicity must have involved a non-linear amplification of the eccentricity cycles though different processes such as the increase in the size of ice volume (Clark et al., 2006; Abe-Ouchi et al., 2013), the influence of sea ice (Gildor and Tziperman, 2001), or the combination of several obliquity (Huybers and Wunsch, 2005) or precession cycles (Cheng et al., 2016; Hobart et al., 2023).

The MPT has been defined as a long-term interval (ca. 1250–600 kyr) in which glacial periods started to become longer, more asymmetric, and severe (Clark et al., 2006; McClymont et al., 2013). An important step during this transition is centered at 900 ka, for which it has been proposed that Antarctic ice volume increased, lowering sea level and allowing for further growth of Northern Hemisphere ice sheets (Elderfield et al., 2012; Mudelsee and Schulz, 1997; Raymo et al., 2006). The MPT also shows an outstanding switch point at ~ 650 ka, when the North American ice sheets coalesced and the instabilities in the Laurentide ice sheet started to produce the Hudson-derived Heinrich events that characterized the following glacial periods (Hodell et al., 2008; Hodell and Channell, 2016). After the MPT, a new climatic step, the mid-Brunhes event (MBE, centered at ~ 430 ka), has been defined as a shift towards warmer interglacial periods with higher sea levels and pCO_2 concentrations (Jansen et al., 1986; Lang and Wolff, 2011; Barth et al., 2018) but with a variable regional expression (Candy and McClymont, 2013; McClymont et al., 2013). The MBE has also been associated with a period of high dissolution in the deep ocean that corresponds to an increase in coccolithophore calcification (Barker et al., 2006; Flores et al., 2003; Hodell et al., 2003; Saavedra-Pellitero et al., 2017; González-Lanchas et al., 2023) and also to periods of intense carbonate production in the shallow carbonate banks and platforms (Droxler et al., 1990; Zeigler et al., 2003). The continental records indicate that the MBE brought wetter and warmer interglacial periods (Candy et al., 2014; Zhisheng et al., 2015). In particular, the loess records indicate an intensification of Asian monsoon precipitation since Marine Isotope Stage (MIS) 13 (Sun et al., 2006). Moreover, the period between the MPT and the MBE represents an important step in human evolution which has been related to this climatic transition with the development of tool innovations, more social interactions, and diversification of human lineages/species (Davis and Ashton, 2019; Moncel et al., 2020, 2015; Galway-Witham et al., 2019; Ao et al., 2020).

The sea-level fluctuations produced by the glacial–interglacial climate variability directly affect the growth and demise of carbonate platforms because the reef environments are sensitive to changes in the bathymetry. In modern carbonate platforms, aragonitic corals and green algae (such as *Halimeda*) are the most common carbonate producers of high Sr aragonite-rich carbonate (HSAC) sediments, whereas calcite producers, such as foraminifers and coccolithophores, are more common in pelagic sediments (Schlanger, 1988; Droxler et al., 1988; Schlager et al., 1994). Variations in carbonate production in tropical platform environments have traditionally been linked to sea level, with high production related to highstands (Schlager et al., 1994; Schlager, 2003). Sea-level fluctuations influenced the carbonate mineralogy of the slope and basin periplatform sediments through alternately flooding and exposing the shallow bank tops where HSAC is produced (Droxler et al., 1983; Boardman et al., 1986; Paul et al., 2012). Bank-derived fine sediments, which are rich in Sr, increased in periplatform sediments during sea-level highstands, when carbonate platform flat tops were flooded and their production and export of carbonate reached their maxima. Conversely, the production and export of those HSAC fine sediments was strongly reduced during sea-level lowstands, when platform tops are exposed and karstify.

The modern ocean is enriched in Sr mainly through riverine and hydrothermal input. Stabilization from aragonite to calcite during sea-level lowstand periods also provides Sr to the ocean, modifying the seawater Sr/Ca ratio (Stoll and Schrag, 1998). Seawater Sr/Ca ratios are not constant globally but regionally variable (Lebrato et al., 2020); however, the mean residence times of Sr and Ca in the ocean, ~ 5 and ~ 1 Myr, respectively (Drever, 1988), allow us to interpret the U1467 Sr/Ca record as changes in the input of different carbonate sources related to regional carbonate production and export processes. The differences in biomineralization between platform and pelagic organisms determine the bulk composition of carbonate sediments in the periplatform areas. The Maldives Inner Sea (Fig. 1) sediment deposition has been shaped by the Indian Ocean currents, forced by monsoonal changes since the middle Miocene (C. Betzler et al., 2016a; Betzler et al., 2018, 2009), similarly to other carbonate platforms (Betzler and Eberli, 2019). The South Asian monsoon (SAM) generates in the northern Indian Ocean, seasonally reversing winds and shifts in the ocean currents re-

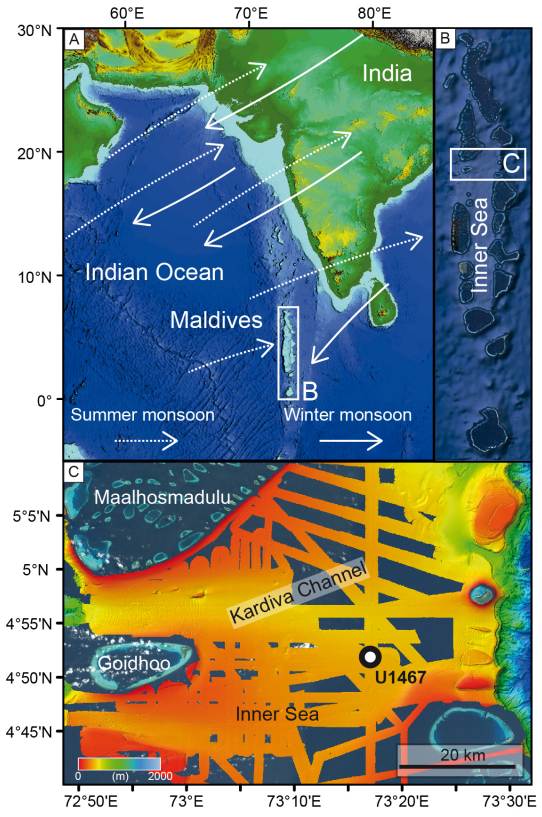

Figure 1. **(a)** Location of the Maldives in the Indian Ocean and representation of the wind directions for the South Asian monsoon; **(b)** close-up of the Maldives Archipelago showing the Maldives Inner Sea bounded by a double row of atolls; **(c)** close-up of the study area and the location of Site U1467 in the Maldives Inner Sea. Figure modified from C. Betzler et al. (2016a).

lated to the migration of the Intertropical Convergence Zone (ITCZ) (Gadgil, 2018). The migration of the ITCZ occurs along with the latitudinal variation in the maximum insolation throughout the year. This combination of processes causes differential heating between land and sea that ultimately generates the monsoon dynamics (Gadgil, 2003; Wang, 2009). In general, during the summer monsoon (June to September), SW winds prevail bringing precipitation over South Asia and promoting the flow of the Southwest Monsoon Current, whereas during the winter season (November–April), NE winds promote the flow of the North Equatorial Current westwards (Tomczak and Godfrey, 2003). During the intermonsoon seasons, particularly in October–November, intense westerly winds, the Indian Ocean equatorial westerlies (IEW) or Wyrtki jets, develop in the equatorial region (Wyrtki, 1973). Those westerly winds introduce strong currents into the Maldives Inner Sea and produce intense mixing of the upper water column. Primary productivity in the Maldives Inner Sea is higher at the end of the summer monsoon season (September–October), when strong IEW produce intense mixing in the upper water column (Schulte et al., 1999; Antoine et al., 1996). The productivity in this region is moderate compared to the primary production that takes place in the western Arabian Sea upwelling region during the summer monsoon season because the wind-driven upwelling effect in the Maldives Sea is counterbalanced by the formation of a low-salinity surface layer that results from local summer rainfall and the inflow of low-salinity waters from the Bay of Bengal (Schulte et al., 1999). A deepening of the mixed layer can also be observed during the winter monsoon but the inflow of low-salinity waters from the eastern Indian Ocean and Bay of Bengal also prevents strong primary productivity (Schulte et al., 1999).

The general atmospheric circulation of the equatorial Indian Ocean develops a west-to-east circulation pattern, following the sea-surface temperature (SST) gradient (cooler in the western region than in the eastern region), which brings precipitation to the southeastern Indian Ocean, off Sumatra (Webster et al., 1999; Saji et al., 1999). However, this atmospheric pattern may fluctuate depending on the SST anomalies of the Indian Ocean dipole (IOD, Fig. 2). The IOD is a coupled ocean–atmosphere phenomenon, similar to the El Niño–Southern Oscillation, which reflects changes in the east–west Indian Ocean SST gradient and in the location of rainfall (Cai et al., 2012; Saji et al., 1999). During negative IOD conditions, the east–west decreasing SST gradient is enhanced, with cooler-than-normal SST in the western part of the basin and warmer-than-normal SST in the eastern part. This configuration leads to intense precipitation in SE Asia and Australia, and intensification of the IEW, which induces strong mixing in the Maldives Sea and high primary productivity (Hastenrath et al., 1993; Marchant et al., 2007; Saji et al., 1999). During a positive IOD phase, the normal SST gradient is reversed, with warmer-than-normal SST in the western part of the Indian Ocean and cooler-than-normal SST in the eastern part (Fig. 2). This configuration results in enhanced precipitation in East Africa and southern India, and weak or reversed IEW, which reduces water column mixing and primary production at the Maldives region.

In this study, we used elemental geochemical compositional records, obtained by X-ray fluorescence (XRF) core-scanning, from International Ocean Discovery Program (IODP) Site U1467 to investigate how sea level and coupled ocean–atmosphere dynamics affected the production and export of carbonate platform sediments to the Maldives Inner Sea over the last 1.3 Myr. Following the hypothesis of sea-level highstand shedding of carbonate platforms proposed by Schlager et al. (1994), we use the Sr/Ca record as a proxy for neritic carbonate production at the Maldives platform and its export to the periplatform sediments (i.e., mix of platform-derived input and pelagic input). According to this hypothesis, high Sr/Ca values in the Maldives Inner Sea are linked to sea-level highstand conditions (high input of Sr-rich platform sediments due to the development of the carbonate factories in the atolls) and low Sr/Ca values are linked to sea-level lowstand conditions (Droxler et al., 1990; Paul et al.,

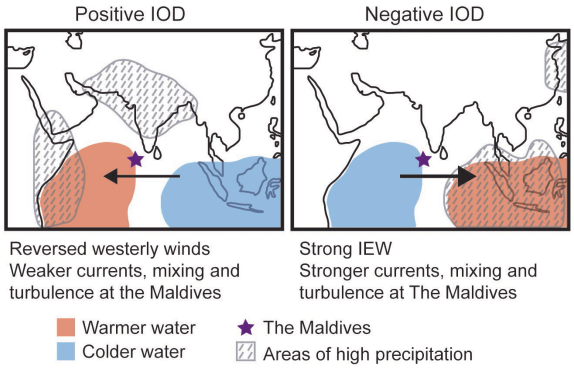

Figure 2. Indian Ocean dipole (IOD) modes (figure modified from Alonso-Garcia et al., 2019). The sketch shows how IOD shifts precipitation in the different regions of the northern Indian Ocean and also how this phenomenon affects water column mixing and productivity at the Maldives Sea. Distribution of sea-surface temperature and precipitation compiled from Marchant et al. (2007), Hastenrath et al. (1993), and Saji et al. (1999).

2012; Betzler et al., 2013; Boardman et al., 1986). The Sr/Ca record has been combined with the Br-normalized record, as a proxy for organic matter content linked to pelagic primary productivity and water column mixing, and with other proxies from Site U1467 that indicate variations in the monsoon dynamics, such as the Fe/K ratio as a proxy for summer monsoon intensity and the Fe input for winter monsoon intensity (Kunkelova et al., 2018). The combination of all those proxies suggests that during the last 1.3 Myr, changes in the carbonate production and export in the Maldives region responded to sea-level variations but also to climate fluctuations related to monsoon dynamics. Moreover, the long-term patterns observed in the records appear to be related to the MPT and MBE events.

2 Geological setting

The Maldives Archipelago (Fig. 1), situated in the central equatorial Indian Ocean, is a 3 km thick isolated tropical carbonate edifice located southwest of India (Aubert and Droxler, 1996; Purdy and Bertram, 1993). The carbonate platform was established on an early Paleogene (60 to 50 Ma) faulted volcanic basement (Duncan and Hargraves, 1990). However, carbonate drift deposition in the Maldives Archipelago only started around 13 Ma (Betzler et al., 2009, 2013, 2018; Betzler et al., 2016a, b) coincident with a partial drowning of the Maldives carbonate platform (Betzler et al., 2009, 2013; Reolid et al., 2019, 2020) and the intensification of the South Asian monsoon in this region (Betzler et al., 2016a; Betzler et al., 2018; Ling et al., 2021; Yao et al., 2023). The water depth at which the drifts were deposited changed through time from ca. 50 m at the time of the first drift deposits around 13–11 Ma (Reolid et al., 2019) to ca. 500 m at present (Betzler et al., 2016a). The sea-level fluctuations that occurred during the Quaternary were recorded as changes in the intensity of the bioturbation (Reolid and Betzler, 2019) and in the fossil assemblages in the drift sediments (Gupta et al., 2010; Bunzel et al., 2017; Sreevidya et al., 2019; Alvarez Zarikian et al., 2022).

The IODP Expedition 359 drilled four holes at Site U1467 in the Maldives Archipelago, Indian Ocean (4°51′ N, 73°17′ E) at an average water depth of 487.4 m. A shipboard composite depth record was established (Betzler et al., 2017) using standard IODP procedures (Correlator software version 2.01.1). High-resolution compositing was based on sediment lightness (L^*) data from holes U1467A to U1467D and adjusted after the cruise based on the higher-resolution X-ray fluorescence (XRF) core-scanning data (Kunkelova et al., 2018). The splice data, including the splice intervals, core offsets, and tie points between each borehole, are archived on the IODP LIMS database (http://iodp.tamu.edu/database/, last access: September 2017). The studied interval corresponds to the uppermost part of the last depositional drift unit (DS10 according to Betzler et al., 2018) and comprises the last 1.3 Myr (from the seafloor to approximately 43 m of composite depth, mcd). The sediment consists of unlithified foraminifer-rich, very fine-to-fine-grained wackestone to packstone texture with a calcareous ooze matrix. The sediment shows periodic changes in the grain size following the glacial–interglacial climatic cycles with finer sediments during interglacial periods (Lindhorst et al., 2019; Alvarez Zarikian et al., 2022). Thick (0.3–1 m) to very thick (> 1 m) intervals defined by color changes ranging from light gray to grayish brown characterize this lithologic unit (Fig. 3a). Bioturbation is common to intense in the darker intervals and is often represented by color mottling. Burrows contain higher concentrations of particulate organic matter and commonly coarser material (Fig. 3a). Contacts between the darker and lighter intervals are gradational. Compared to the dark intervals, light packages appear more bioturbated and are depleted in particulate organic matter (Betzler et al., 2016b, 2018; Reolid and Betzler, 2019). The fossil assemblage consists of abundant well-preserved planktonic foraminifers and pteropods, especially in the uppermost part of the interval (Fig. 3b). Benthic foraminifers, ostracods, mollusk fragments, echinoid fragments, and dark brown organic matter particles are present but not very abundant. In addition, cold-water coral remains were found at 7.13 m below sea floor (m b.s.f.) and 11.90 m b.s.f. (Fig. 3c). The fine fraction is made up of coccoliths, aragonite needles, tunicates, silicoflagellates, and sponge spicules with minor clay minerals and particulate organic matter.

3 Materials and methods

Non-destructive XRF analyses were performed at the Ocean Drilling and Sustainable Earth Science (ODASES) core scanning facility at the IODP Gulf Coast Repository (GCR)

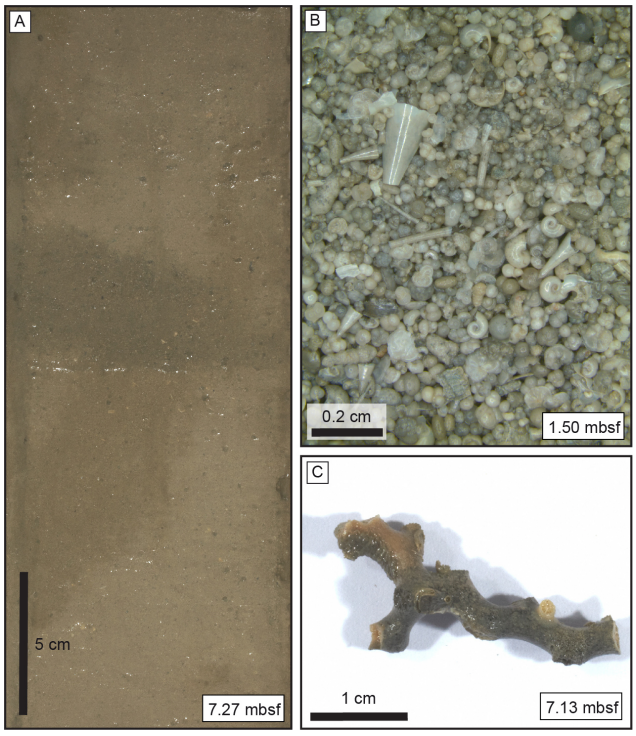

Figure 3. Facies and bioturbation of the sheeted drift deposits at Site U1467 (modified from Reolid and Betzler, 2019). **(a)** Core photograph of an unlithified wackestone with large trace fossils (possibly *Thalassinoides*); **(b)** photomicrograph of a grainstone from the uppermost part of the drift with abundant pelagic fauna including planktonic foraminifera and pteropods; **(c)** fragment of the cold-water coral *Lophelia Pertusa*.

at Texas A&M University (USA), using a third-generation AvaaTech XRF scanner configured to analyze split sediment core halves for elements between Mg and U in the periodic table (Lyle and Backman, 2013). Data were acquired with a Canberra X-PIPS silicon drift detector (SDD) with 150 eV X-ray resolution at 5.9 keV and a Canberra Digital Spectrum Analyser model DAS 1000. The X-ray source was an Oxford Instruments 100 W Neptune X-ray tube with a rhodium (Rh) target. Raw spectral data were processed using the Canberra WINAXIL software package to produce elemental intensity data. The dual slit system was set to provide down-core spatial resolution of 10 mm and cross-core spatial resolution of 12 mm. The system performed two consecutive runs of the same section, the first one at 9 kV, 0.25 mA, and 6 s (for elements such as Ca, Fe, K, Al, and Ti) and the second one at 30 kV, 1.25 mA, and 6 s (for elements such as Sr, Br, Rb, and Fe). Each core section was removed from refrigeration at least 2 h before scanning, scraped to clean and smooth the core surface, and covered with 4 µm thick Ultralene plastic film to prevent contamination of the X-ray detector. Measurements were taken at 3 cm intervals whenever possible. Some measurements were skipped or shifted to the nearest suitable area in order to avoid bad performance of the detector on cracks or uneven surfaces.

To evaluate the reliability of the XRF scanning records, Kunkelova et al. (2018) and Carrasqueira et al. (2023) performed quantitative XRF measurements in selected samples, showing a good match between the methodologies. In Kunkelova et al. (2018), the correlation coefficient between the types of measurements was good for Fe (0.8) and robust for K and Si (0.9). However, for elements like Ti, in rather small concentrations in the sediment, the correlation was low (0.2), indicating low reliability for this element in the XRF-scanning records. In Carrasqueira et al. (2023), correlation coefficients were even higher for Fe ($r = 0.94431$), similar for K ($r = 0.89381$) and Si ($r = 0.86234$), and slightly higher for Ti ($r = 0.67319$) than in Kunkelova's work. Carrasqueira et al. (2023) also calculated the correlation for Sr ($r = 0.94054$). Those results indicated that the XRF-scanning records are robust indicators of the sediment concentration of the elements displayed in this article. To reduce the effects of water content, porosity, and lithological variability (Tjallingii et al., 2007), the results of the XRF scanning have been normalized dividing the raw total counts of each element by the total counts for each sample measured excluding Ag and Rh. When elements are not plotted in ratios they are shown as normalized, for instance Fe_n means Fe record was normalized versus the total counts. In this study, following Aitchison (1982), the Sr/Ca and Fe/K ratios were normalized using natural logarithm of the ratio, whereas the Fe/K ratio published in Kunkelova et al. (2018) was a simple ratio between the element intensities.

Principal component analysis (PCA) and Pearson's correlation were performed using PAST software (Hammer et al., 2001) with the matrix of the XRF scanning normalized element intensities. In order to identify long-term changes in the XRF records, we computed the cumulative sum (CuSum) of the deviations from the mean for Fe_n, Fe/K, and Sr/Ca records. The cumulative sum method was developed for industrial control to detect changes in sequential production (Page, 1954), but it has been extensively applied in biological oceanography (Ibanez et al., 1993; García-Comas et al., 2011). The cumulative sum of a record (i.e., a linear sequence) shows each value with respect to the long-term average. A positive slope shows a period of values greater than the long-term average, and a negative slope shows a period of values smaller than the long-term average. The steepness of the slope reflects how different a period is from the long-term average. Those changes in the tendency (that is, sequential periodical changes in the slope) can be interpreted as periodical changes in the environmental conditions related to each proxy. For example, the changes in the tendency of different ratios have been interpreted as changes towards drier or humid conditions in previous work with XRF-scanning records (Caley et al., 2018).

The chronology of the studied interval of Site U1467 was performed correlating the Fe- and K-normalized records

from the XRF scanning with the benthic $\delta^{18}O$ records of ODP Sites 967–968 (Konijnendijk et al., 2015) and the "Prob-stack" of Ahn et al. (2017). This correlation was performed using QAnalyseries (Kotov and Pälike, 2018); it is based on the strong response of Fe and K (as humidity proxies) to glacial–interglacial variability and has been previously used in Alonso-Garcia et al. (2019) and Alvarez Zarikian et al. (2022), showing an excellent agreement with the benthic $\delta^{18}O$ age model of Stainbank et al. (2020). The age / depth table for all tie-points is included in the Supplement.

4 Results

4.1 Geochemical data

4.1.1 Sr/Ca

The lnSr/Ca obtained from the XRF-scanning for the study interval displays values ranging from a minimum of −0.144 to a maximum of 0.054 (Fig. 4e). The fluctuations in this ratio show a cyclical pattern that follows the glacial–interglacial cycles observed in the benthic $\delta^{18}O$ stack (Ahn et al., 2017), as well as interstadial–stadial events that can be observed in the Fe-normalized record (Fig. 4b) or in the benthic $\delta^{18}O$ record of the same site (Fig. 4a, Stainbank et al., 2020). PCA and Pearson's correlation show that the Sr record is positively correlated to Ca ($r = 0.71$, $n = 2356$) and negatively correlated to Fe ($r = -0.97$) and K ($r = -0.88$). Sr/Ca and Fe_n show rather high negative correlation ($r = 0.84$).

Minimum values in Sr/Ca occurred during cold periods, whereas maximum values are associated with warm intervals. Among all the interglacial intervals, MIS 11 stands out with maximum values, followed by other interglacials such as MIS 5, MIS 1 (The Holocene), MIS 17, MIS 13, and MIS 31. Maximum values in Sr/Ca also align well with periods of high sea levels (Fig. 4) based on the comparison with the sea-level reconstruction of ODP Site 1123 (east of New Zealand, Elderfield et al., 2012) and the global sea-level stack of Spratt and Lisiecki (2016). However, a comparison in a cross-plot between the IODP Site U1467 Sr/Ca record and the ODP Site 1123 sea-level record indicates low correlation between the proxies (Fig. 5). Indeed, this can be observed if we examine the records carefully. For example, in the early part of the record (interval from 1050 to 900 ka) some of the interglacial periods present rather high sea levels but moderate Sr/Ca values, whereas intervals with moderately high sea-level values, such as MIS 13 or 5, show rather high Sr/Ca values.

4.1.2 Br

The Br-normalized record (Br_n) obtained from the XRF-scanning for the study interval ranges from a minimum of 0.007 to a maximum of 0.0327 (Fig. 6b). Br values are consistently high during glacial periods and reach their minimum values during the optima of the interglacial periods with a sharp change from high to low values during Terminations. The transition from interglacial to glacial periods may be gradual in the Br record but most of the transitions towards glacial periods show an abrupt increase in Br values. The maximum value corresponds to the Last Glacial Maximum, whereas the minima values correspond to MIS 31. PCA and Pearson's correlation indicate that the Br record is positively correlated to Fe ($r = 0.79$, $n = 2356$) and K (0.71), but it is negatively correlated to Ca ($r = -0.71$) and Sr ($r = -0.85$). Results of Sr/Ca compared to other monsoon proxies (Kunkelova et al., 2018) and Br are shown in Fig. 6, and a close-up of interglacial periods MIS 5, 11, and 13 is shown in Fig. 7. Figure 7 shows the good coherence between the Br and Fe records across different interglacial periods.

4.2 Cumulative sum analysis

The CuSum values of the U1467 Sr/Ca record show three different trends over the studied interval, indicating changes in the export and production of HSAC just at the MPT and MBE (Fig. 8). Before the MPT the HSAC production was lower than the average; between MPT and MBE the production of HSAC was average; and after the MBE there was an increasing trend that indicates the HSAC production was above average. The CuSum values of the U1467 Fe record also show two changes with the same timing as in the Sr/Ca record. However, in the Fe record the trend is only increasing the steepness of the gradient, indicating higher Fe (dust) input after the MPT and even greater after the MBE (Fig. 8). The CuSum of the Fe/K ratio record shows a similar trend to Fe, with an increase towards drier conditions after the MPT.

5 Discussion

5.1 Carbonate production and sea-level oscillations

The Maldives Inner Sea has been functioning as a natural sediment trap (Belopolsky and Droxler, 2003; Betzler et al., 2009). It receives terrigenous sediments of aeolian origin (Kunkelova et al., 2018; Lindhorst et al., 2019; Yao et al., 2023; Carrasqueira et al., 2023), fragments of shallow-water organisms populating the atolls surrounding it, and planktonic and benthic pelagic microorganisms (Gupta et al., 2010; Betzler et al., 2016b, 2018; Bunzel et al., 2017; Sreevidya et al., 2019; Bialik et al., 2020; Alvarez Zarikian et al., 2022). Fluctuations in the input of the different carbonate components (mainly foraminifers and coccolithophores versus aragonitic pelagic and shallow-marine organisms) influences the Sr content of the pelagic sediments of the Maldives Inner Sea. During sea-level highstand periods, carbonate production at the platform top is at a maximum (Betzler et al., 2013), sequestering large amounts of carbonate and producing a shelf-basin fractionation that drives dissolution in the deep basins due to the increase in the carbonate compensa-

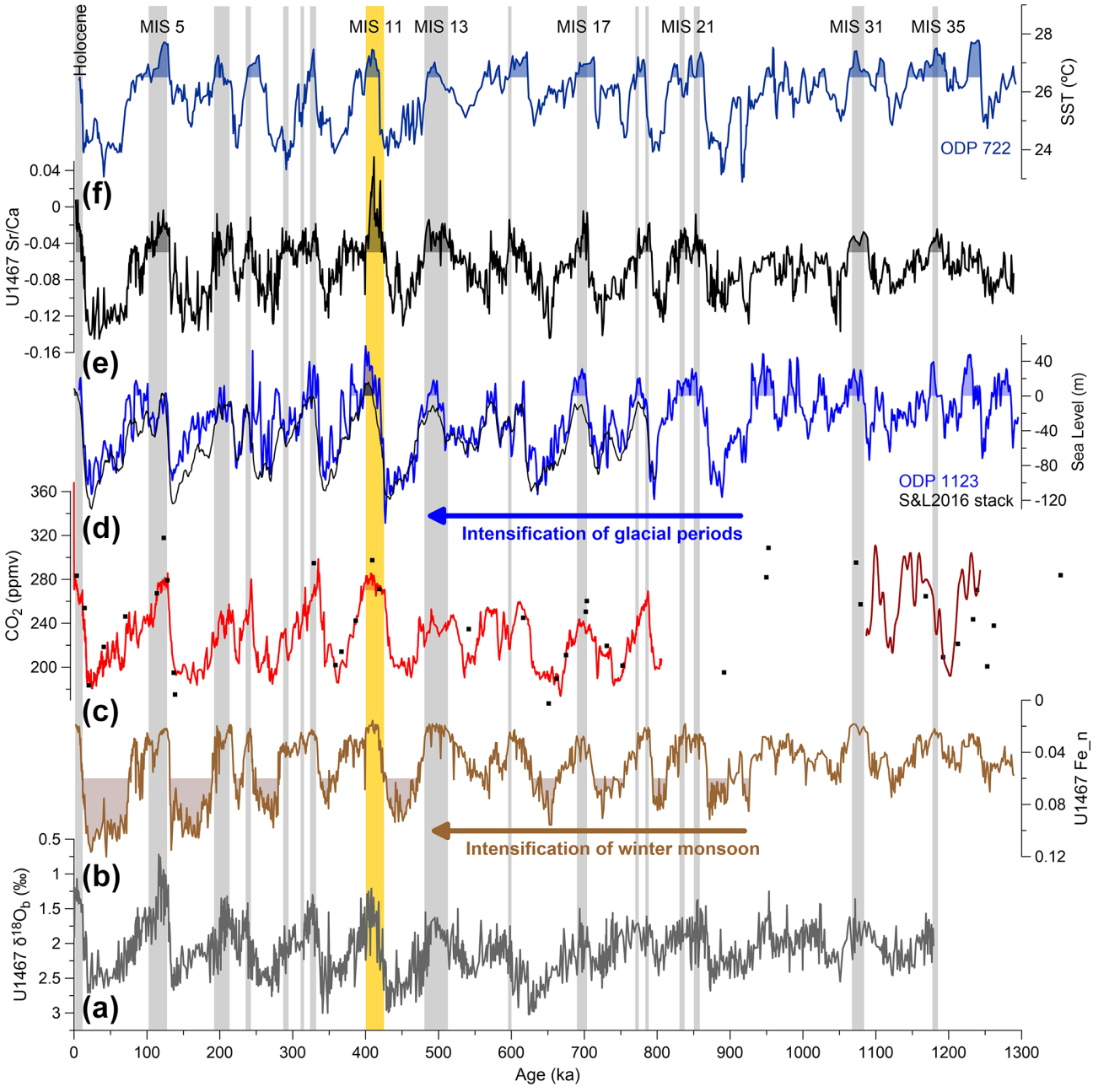

Figure 4. XRF data from U1467 compared to other records. **(a)** Benthic foraminifer $\delta^{18}O$ record of Site U1467 (Stainbank et al., 2020) for stratigraphic reference; **(b)** Fe-normalized record from U1467 XRF data; **(c)** CO_2 records for the last 1.3 Myr, light red line showing data from EDC3 (Bereiter et al., 2015), dark red line showing data from Chalk et al. (2017), and black squares showing data from Honisch et al. (2009); **(d)** sea-level reconstructions from Elderfield et al. (2012) and Spratt and Lisiecki (2016); **(e)** Sr/Ca record from U1467; **(f)** sea-surface temperature (SST) from ODP 722 in the Arabian Sea (Herbert et al., 2010). Periods of high Sr/Ca values are highlighted by vertical gray bands except for MIS 11, which has been highlighted in orange.

tion depth (Hodell et al., 2001; Zeigler et al., 2003). The Sr-rich carbonate that forms in the atolls is transferred to the pelagic sediments of the Maldives Inner Sea due to storms, ocean currents, and tidal erosion of the carbonate banks. During all interglacial and interstadial events, the shallow-water marine-derived sediments accumulate in the pelagic environment (Fig. 9a), increasing the U1467 Sr/Ca values (Fig. 4). In addition, high temperature and changes in currents may also promote the abiotic formation of HSAC on the shallow platforms due to local supersaturation and may also increase the export of HSAC to the periplatform (Purkis et al., 2017; Bialik et al., 2022). Conversely, during times of sea-

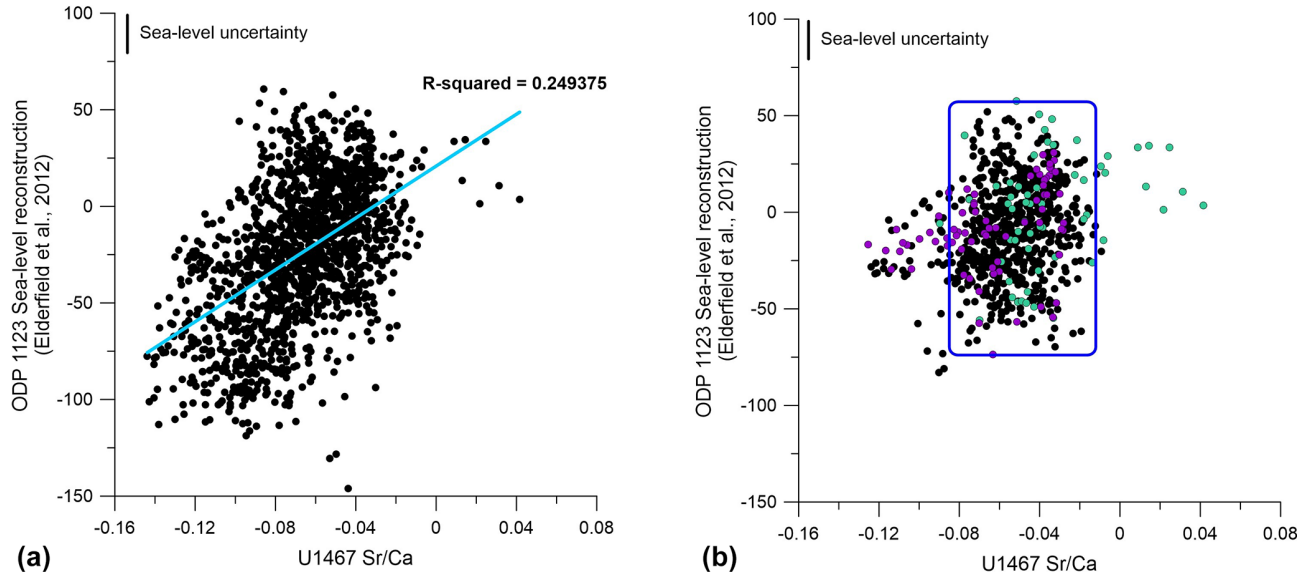

Figure 5. Cross-plot between U1467 Sr/Ca and the ODP 1123 sea-level record (Elderfield et al., 2012). Panel **(a)** shows the full dataset comparison including glacial and interglacial periods and the regression line with the R^2 correlation value. Panel **(b)** shows only interglacial data: green dots correspond to MIS 11 and purple dots to MIS 31, two periods with strong HSAC deposition. Blue rectangle indicates where most of the interglacial data are grouped. Sea-level uncertainty for the ODP 1123 sea-level record is ± 20 m (Elderfield et al., 2012).

level lowstands, the demise of carbonate production at the platform top, and the fact that lower sea levels prevent wave erosion of the carbonate platforms, decreased the input of sediments of platform origin (atolls and upper slope) to the pelagic deposits (Fig. 9b). Consequently, a reduction in the Sr/Ca values in the periplatform sediments can be observed (Fig. 4).

There is a clear correspondence between the long-term sea-level oscillations (observed at the reconstructions from east of New Zealand, ODP Site 1123, by Elderfield et al., 2012, and global stack by Spratt and Lisiecki, 2016) and the U1467 Sr/Ca record of the last 1.3 Myr (Fig. 4). This suggests that long-term sea-level oscillations controlled the carbonate production in the atolls. Enhanced carbonate production and sediment export from the Maldives atolls occurred during intervals with sea level similar to or higher than the Holocene level, particularly associated with the optimum phase of interglacial/interstadial periods (Fig. 7). It is important to note that the uncertainty in the sea-level estimates used in this work is ± 18–24 m (2σ error) for the global stack by Spratt and Lisiecki (2016) and ± 20 m for the ODP Site 1123 record (Elderfield et al., 2012). Indeed, it has been suggested that some interglacial periods, such as MIS 11 are overestimated in the Elderfield et al. (2012) record compared to other publications, which suggest between 20 and < 13 m over present sea level (Raymo and Mitrovica, 2012; Olson and Hearty, 2009; Hearty et al., 1999). Although a better precision would be desired for the comparison with the U1467 Sr/Ca record, at the moment, these are the best long-term records we can use, and besides the high uncertainties, the Elderfield et al. (2012) record shows a good match with the sea-level estimates from coral reefs for the last 250 kyr (for more details see Fig. S6 from that publication).

Despite the uncertainties in the sea-level reconstructions, and the minimal age model differences that may occur between Site U1467 and the sea-level records, it is noteworthy that carbonate production and its export from the Maldives atolls (recorded as high Sr/Ca values in U1467) was rather active throughout most of the interglacial maxima for the last 1.3 Myr. The only exception is the interval between MIS 29 and MIS 25 (∼ 1030–942 ka), in which the sea-surface temperatures of the northern Indian Ocean were also slightly lower (Herbert et al., 2010). However, the comparison of Sr/Ca and sea-level records in a cross-plot (Fig. 5) shows low correlation ($R^2 = 0.25$) and particularly high dispersion of the values during interglacial periods (Fig. 5b). This indicates that sea level controls the platform growth to some extent, but the elevation of sea level is not proportional to the carbonate production and sediment export. Once a certain sea-level threshold is reached and the carbonate production in the atolls is established, there must be other factors impacting the HSAC production and export from the Maldives platforms to the inner sea. On the following sections, we will discuss other environmental controls for the production and export of HSAC.

5.2 Carbonate production and monsoon dynamics

The carbonate producers within the carbonate factories, including coral reef communities and other organisms living in the atolls, are highly sensitive to sea-surface temperature

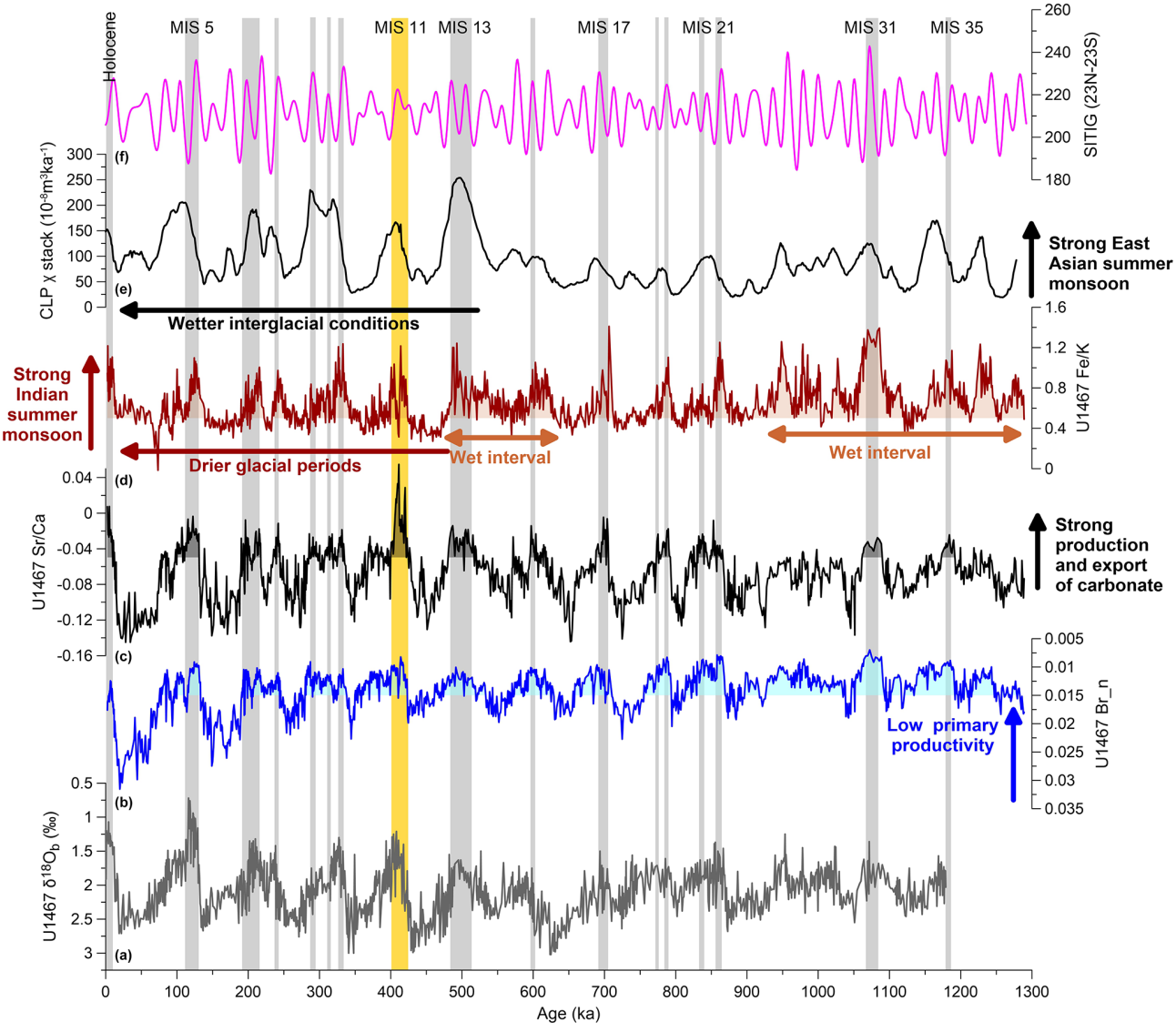

Figure 6. Monsoon and productivity proxies: **(a)** benthic foraminifer δ^{18}O record of Site U1467 (Stainbank et al., 2020) for stratigraphic reference; **(b)** Br-normalized record of U1467 as a proxy for primary productivity; **(c)** Sr/Ca record from U1467 as a proxy for carbonate production and export at the Maldives platforms; **(d)** Fe/K ratio of U1467 as a proxy for summer monsoon intensity (Kunkelova et al., 2018); **(e)** Chinese Loess Plateau magnetic susceptibility (χ) stack, as a proxy for East Asian summer monsoon, from Ao et al. (2023); **(f)** summer intertropical insolation gradient (SITIG) between 23° N and 23° S (Laskar et al., 2004). Periods of high Sr/Ca values are highlighted by vertical gray bands except for MIS 11 which has been highlighted in orange.

and to the input of nutrients (Hallock and Schlager, 1986; Hallock, 2005). Coral reefs mostly live in warm and oligotrophic environments. The increase in nutrients stimulates plankton growth, reducing the transparency of the water and limiting coral and calcareous algae growth. In the Maldives Sea, SST ranges from 28.0 to 29.7 °C (NOAA Coral Reef Watch site), which is optimum for reef communities, while the input of nutrients (and, as a consequence, the turbidity of the water column) depends on the wind intensity. Stronger winds promote the input of dust and mix the upper water column, bringing nutrients to the surface. The intensity of the winds in this region is controlled by monsoon dynamics and IOD. Positive IOD phases are linked to warmer-than-normal SST in the western Indian Ocean and weak easterly winds (Fig. 2), which modify sea-surface circulation and prolong the Indian summer monsoon season by delaying the southward movement of the ITCZ (Cai et al., 2021). Those conditions are optimal for the development of coral reef communities due to the weaker winds and high SST. Sustained increases in SST may bring punctual bleaching events but coral reefs usually recover rather quickly after them (Kench et al., 2022).

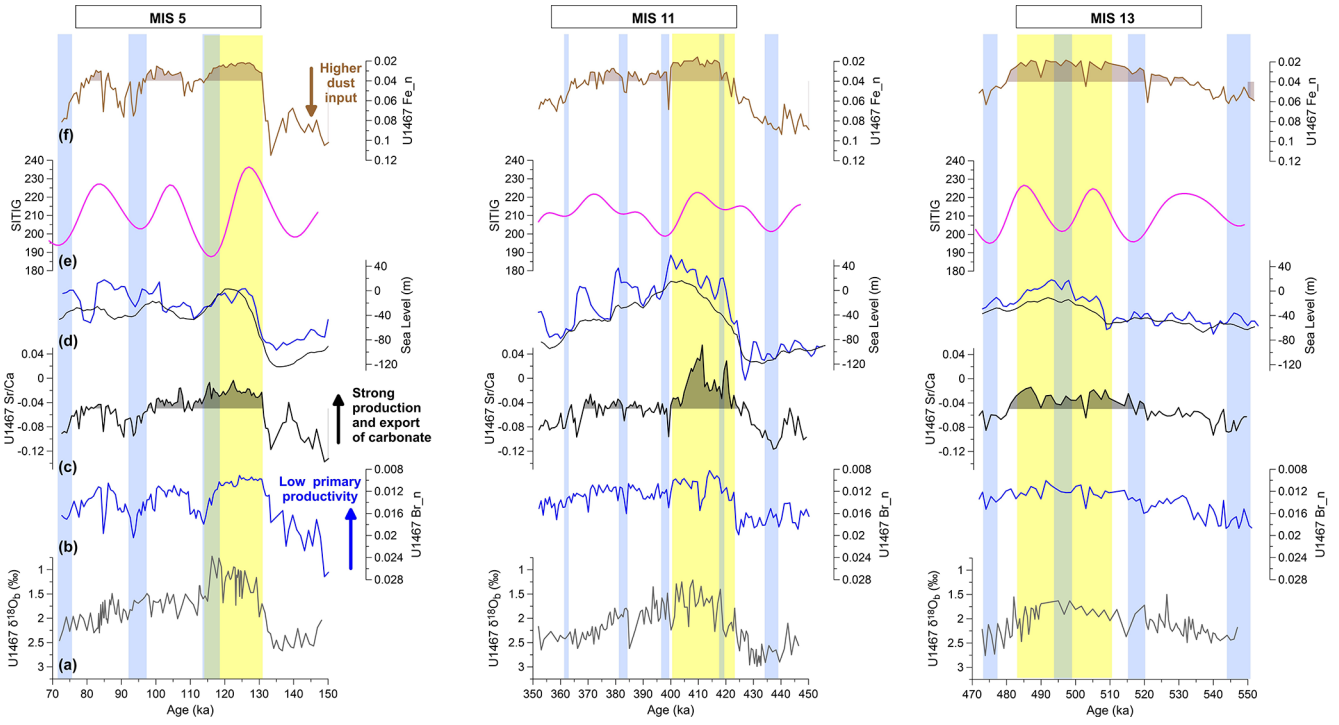

Figure 7. Detailed sequences of the U1467 records of MIS 5, MIS 11, and MIS 13. **(a)** Benthic foraminifer δ^{18}O record of Site U1467 (Stainbank et al., 2020) for stratigraphic reference; **(b)** Br-normalized record of U1467 as a proxy for primary productivity; **(c)** Sr/Ca record from U1467 as a proxy for carbonate production and export at the Maldives platforms; **(d)** sea-level reconstructions from Elderfield et al. (2012) and Spratt and Lisiecki (2016); **(e)** summer intertropical insolation gradient (SITIG) between 23° N and 23° S (Laskar et al., 2004); **(f)** Fe-normalized (Fe-n) record as a proxy for winter monsoon intensity (Kunkelova et al., 2018). Vertical blue bars indicate periods of low SITIG, which are not favorable for platform growth. Vertical yellow bars indicate the main period of carbonate platform production and export.

On the other hand, the negative IOD phases increase the strength of the IEW (Saji et al., 1999), which generates stronger currents, mixing the water column and upwelling nutrients. According to Hallock and Schlager (1986), these conditions produce environmental stress and reduction in coral reef growth. In addition, intensification of the monsoon winds has been related to modification of the atolls' shorelines by erosion (Kench et al., 2005, 2009). Studies on present-day atolls (Kench et al., 2009; Gischler et al., 2014) have demonstrated how yearly variations in the monsoon intensity, wind, and waves modify the circulation pattern of surface currents and, accordingly, the erosional balance of the atolls. It is reasonable to suppose that, in the past, the Maldives atolls, which developed soil and vegetation as their modern counterparts, were intensely eroded by enhanced monsoonal storm waves and wind-driven currents, modifying the morphology of the emerged areas and exporting sediments towards the surrounding deep-environments. Indeed, the strengthening of the ocean currents and winds has been claimed to be a factor that generated the demise of carbonate platform production in the Maldives during the Late Miocene (Betzler et al., 2009, 2013).

5.3 Dust input and pelagic primary productivity

The Fe-n record of U1467 is mainly related to the aeolian dust input from the continent and, therefore, to the strength of winter monsoon (Kunkelova et al., 2018). Clays and quartz that arrive in the Maldives Inner Sea are mainly related to aeolian input because the elevation of the Maldives Archipelago prevents most of the entrance of riverine input from either the Arabian Sea or the Bay of Bengal (Kolla et al., 1981). Even though the freshwater plumes of the Ganges and Brahmaputra rivers could transport large amounts of sediments, the oceanographic configuration of the surface currents in the northern Indian Ocean only allows freshwater transport from the Bay of Bengal during the winter, when the river discharge is minimal (Hormann et al., 2019). The compilation of aerosol distribution from 2020 Copernicus Atmosphere Monitoring Service (CAMS) global Atmospheric Composition Reanalysis 4 (Inness et al., 2019) and the aerosol optical depth from NASA (https://earthobservatory.nasa.gov/global-maps/MODAL2_M_AER_OD, last access: September 2019) indicates that most of the aeolian input of sediments reach the Maldives Archipelago during the winter monsoon (Kunkelova et al., 2018, 2022). Finding a proxy

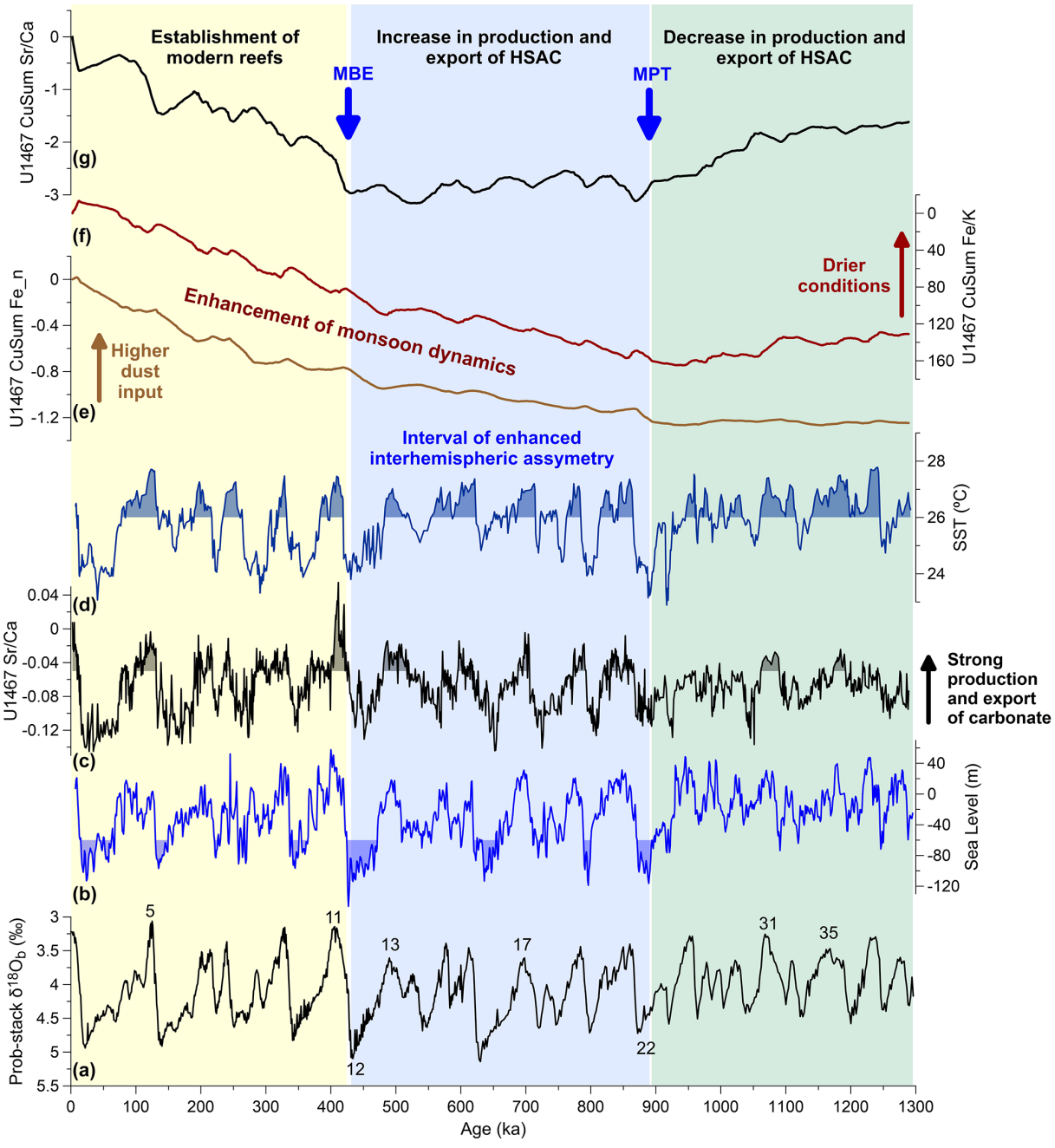

Figure 8. Identification of different phases in the platform growth and monsoon dynamics using the cumulative sum (CuSum) trends. **(a)** Prob-stack benthic foraminifer δ^{18}O record (Ahn et al., 2017) for stratigraphic reference; **(b)** sea-level reconstructions from Elderfield et al. (2012) and Spratt and Lisiecki (2016); **(c)** Sr/Ca record from U1467 as a proxy for carbonate production and export at the Maldives platforms; **(d)** sea-surface temperature (SST) from ODP 722 in the Arabian Sea (Herbert et al., 2010); **(e)** CuSum of Fe-n record; **(f)** CuSum of Fe/K record; **(g)** CuSum of Sr/Ca record. Green shading indicates the pre-MPT interval, blue the period between MPT and MBE, and yellow the period after MBE.

to differentiate between aeolian and riverine input for the U1467 record has not been possible with the XRF-scanning data since Ti concentration in the sediment is very low and Zr was not reliable because the Sr K-beta peak (15.835 kV) overlaps the Zr K-alpha peak (15.775 kV).

The U1467 Fe/K record was interpreted as a proxy for summer monsoon intensity by Kunkelova et al. (2018) since chemical weathering in South Asia dominates under humid conditions, leading to high Fe/K values, whereas mechanical weathering dominates under dry conditions, leading to low

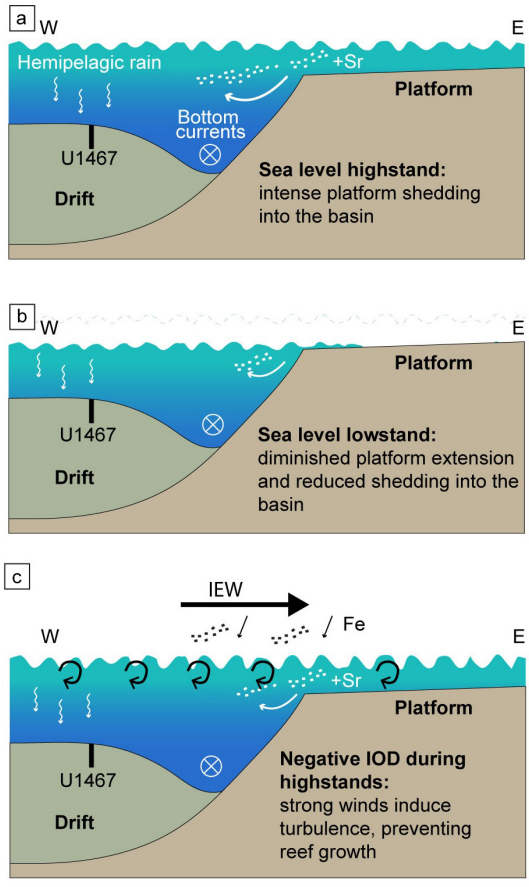

Figure 9. Sketch depicting the main factors controlling the production of carbonate in the atolls and its export. **(a)** Sea-level highstand and optimum conditions for carbonate production at the Maldives atolls; **(b)** sea-level lowstand drives the lowest carbonate production and export due to lower sea level; **(c)** carbonate production during highstands but under negative IOD that reduces carbonate production.

Fe/K values (Govin et al., 2012). Regardless of the aeolian or riverine origin of the siliciclastic elements, the interpretation of the Fe/K record as a proxy for mechanical versus chemical weathering would be the same because the main source of the detrital elements is the Indian Peninsula at any case. Therefore, the Fe/K record reflects if the region of the Indian Peninsula was affected by a wetter or drier climate either through aeolian or riverine input of Fe and K.

The comparison of U1467 Sr/Ca and Fe-n records shows that rather high values of Sr/Ca occurred simultaneously with low Fe input to the Indian Ocean (Fig. 4). Fe input to the Maldives Sea increased during the glacial periods of the MPT along with the intensification of the global glacial conditions. It has been calculated that the generally colder and drier glacial conditions resulted in an increase in dust fluxes by a factor of 2–5 (Maher et al., 2010). The MPT aridification of the South Asian region was augmented during glacial periods, increasing glacial dust export (Kunkelova et al., 2018). This input of dust increases the turbidity of the water, preventing the growth of the platform top carbonate factory. The U1467 Fe/K record (Fig. 6d) indicates an increase in chemical weathering (i.e., in humidity) in the Indian continent after each termination, with particularly humid conditions during MIS 31 and during late MIS 13. Similar alternations between dry and wet conditions in South Asia have been described in other studies, indicating that the displacement of the ITCZ controls the precipitation in South Asia at glacial–interglacial timescales (Zhisheng et al., 2011; Ao et al., 2023; Carrasqueira et al., 2023) but also at millennial scales (Ota et al., 2022). The Sr/Ca record shows increases in the carbonate production and export at times of increases in the Fe/K ratio, indicating the influence of summer monsoon conditions in the development of the carbonate factory.

Changes in pelagic primary productivity have been inferred in this study with the Br-n record (Fig. 6b), following previous work in this region (Bunzel et al., 2017; Ziegler et al., 2008). The link between the monsoon intensity and surface water productivity in the Maldives Inner Sea was confirmed by Bunzel et al. (2017), who showed how low values of $\delta^{13}C$ in two species of benthic foraminifera indicate enhanced vertical mixing of the water column that increased the supply of nutrients from subsurface waters into the photic zone, enhancing surface water productivity. Pelagic primary productivity was also inferred at Site U1467 using the total alkenone concentration in the sediment samples (Alonso-Garcia et al., 2019; Alvarez Zarikian et al., 2022), although this record only reflects coccolithophore production. Both records indicate that pelagic primary productivity was rather low during the interglacial optima. We acknowledge that since the Br record is a proxy for total organic carbon (TOC) content (Ziegler et al., 2008), the high carbonate export from the platforms may be diluting the overall organic matter content. However, the Br record shows a moderate negative correlation with the Ca record, indicating that carbonate dilution is not the only factor controlling the Br concentration in the sediments. The alkenone concentration record does not follow the Ca record either. It is likely that during the glacial periods, pelagic primary productivity was enhanced due to stronger winds, and probably more phyto- and zooplankton accumulated in the sediments, increasing the accumulation/preservation of organic matter.

Br is more abundant during the glacial periods in the Maldives Inner Sea (Bunzel et al., 2017, and this study), indicating higher organic carbon accumulation. According to Ziegler et al. (2008), total organic carbon (TOC) and Br content in the sediments show a clear correlation except when there is input of terrestrial organic matter. The alkanes record of U1467 does not show a strong correlation with the Br record (Fig. 10); thus, the input of organic matter from the continent does not seem to be the factor controlling the Br variations. In addition, the glacial periods show higher bottom water oxygenation based on the higher plant *n*-alcohols / *n*-alkanes (HPA) ventilation index and the os-

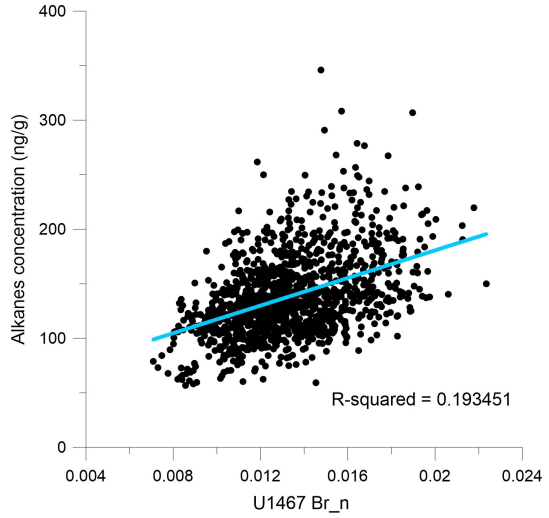

Figure 10. Cross-plot between U1467 Br-normalized record (this study) and the U1467 alkanes concentration in the sediment (Alonso-Garcia et al., 2019, and unpublished data).

tracod assemblages (Alvarez Zarikian et al., 2022). If respiration/degradation of the organic matter was an issue, the glacial periods would be depleted in Br and TOC but it is the opposite. Therefore, we propose that Br variations reflect sea-surface productivity and that the organic matter is not very much affected by diagenetic processes. Enhanced detrital input, including clays, during the glacial periods can also contribute to organic matter preservation. A significant correlation has been described between TOC preserved in the sediments and mineral surface area (mainly controlled by the presence of clay minerals) in modern and past continental margin sediments (Hedges and Keil, 1995; Kennedy et al., 2014).

We suggest that high Br content during glacial periods is the result of higher pelagic primary productivity and lower carbonate export from the shallow-water platform (i.e., the atolls), whereas during interglacial periods, enhanced HSAC production and sediment export of carbonate from the Maldives atolls and lower pelagic primary productivity reduced the Br accumulation in the sediments. The orbital variations observed in the Br record probably correspond to variations in sea surface primary productivity related to orbital parameters, mainly precession and obliquity. The role of fine terrestrial material in the production of shallow-water carbonate material is still poorly understood. In the Bahamas, it was demonstrated that Saharan dust plays a pivotal role in the production of fine carbonate material on the platform (Swart et al., 2014). In the Maldives, the situation appears to be more complex because the Maldives are not nutrient limited during interglacial periods due to the combination of both the input of fine particles from the Bay of Bengal and upwelled waters from the west (Radice et al., 2019). In summary, the obtained Br-n record (Fig. 6) has been interpreted as a record of organic matter accumulation, with low values corresponding to periods of low pelagic primary productivity, concomitant with low dust input and high production and export of HSAC from the platforms.

5.3.1 Variations in SST and monsoon intensity as control of platform sediment export

In order to track changes in the SST of the western Indian Ocean (and thereby, possible changes in the general IOD state), we compared the U1467 XRF scanning elemental records with the SST record of ODP Site 722 (Fig. 4f), in the Arabian Sea (Herbert et al., 2010), which shows higher temperature variability than the U1467 SST record (Alonso-Garcia et al., 2019), and a wider signal than the Maldives Sea. The Sr/Ca record from U1467 indicates that an elevated production and export of HSAC in the Maldives Sea occurred at times when sea level was high (generally similar or higher than at present), SST was warm in the western part of the Arabian Sea (probably warmer than 26.5 °C at Site 722 and even warmer in the Maldives Sea), primary productivity was low (low Br values), and summer monsoon was prolonged driving rather humid conditions in India (high values in the Fe/K record, Fig. 6d) and East Asia (Sun et al., 2022). Interglacial maxima seem to correspond to periods of strong summer monsoon and persistently positive IOD conditions, which would bring warm SST and low mixing and turbidity to the western part of the northern Indian Ocean decreasing the pelagic primary productivity within the Maldives Inner Sea. The lowest values of Br are recorded during these intervals, which also coincide with sea-level highstands and high HSAC export.

Small drops in sea level usually coincide with the intensification of the winter monsoon season (Fe-n record, Fig. 4b), and sharp reductions in the Sr input into the basin. The strengthening of the winter monsoon may have increased the amount of dust delivered to the Maldives augmenting the turbidity in the surface waters and hampering the growth of carbonate platform producers along with the sea-level drop. Consequently, the carbonate export from the atolls was reduced. In addition, pervasive neutral and negative IOD conditions probably generated strong westerly winds in the equatorial region during the inter-monsoon season (Saji et al., 1999; Webster et al., 1999; Cai et al., 2021). This would have contributed to increase the intensity of the sea-surface currents and the mixing of the upper water column, generating more turbidity and also preventing the development of coral reef communities and other carbonate platform producers (Fig. 9c).

Summer monsoon strength and IOD conditions have been linked to the summer intertropical insolation gradient (SITIG) between 23° N and 23° S on 21 June (Reichart, 1997; Mantsis et al., 2014; Bosmans et al., 2015; Alonso-Garcia et al., 2019). The SITIG responds to the differential heating of both hemispheres at low latitudes, and mod-

ern observations suggest that this gradient controls the tropical monsoon (Gadgil, 2003; Webster, 2004). The SITIG record (Fig. 6f) shows a precessional component, although it is largely controlled by obliquity because the tilt of the Earth increases/reduces the seasonal insolation contrast between the summer and winter hemispheres, driving a higher gradient over the tropics during obliquity maxima (Mantsis et al., 2014). High SITIG values occur when the interhemispheric pressure gradient is high, resulting in strong cross-equatorial winds and moisture transport into the summer hemisphere, associated with an intensified winter Hadley cell in the Southern Hemisphere and a latitudinal migration of the ITCZ towards the warmer hemisphere (Reichart, 1997; Mantsis et al., 2014; Bosmans et al., 2015), which increases precipitation over Asia (Beck et al., 2018).

Increases in the humidity in South Asia, recorded by the U1467 Fe/K ratio, are coetaneous with high SITIG values, particularly during interglacial periods (Fig. 6). Moreover, increases in the U1467 Sr/Ca also coincide with high SITIG values, which indicates that this parameter may be controlling the development of the carbonate factory through its influence on the summer monsoon. Obviously, sea level is the main factor controlling the production and export of HSAC in the Maldives Sea, but high SITIG and the development of positive IOD seem to favor the growth of the coral reef communities and other carbonate producers at the atolls as it can be observed in the detailed sequences of MIS 5, MIS 11, and MIS 13 (Fig. 8). The close-up of these three interglacial periods, although with probably some age uncertainty, shows that even though sea level may be relatively high, if the SITIG is not high, dust input increases and the development of the atoll's communities is reduced, decreasing the Sr/Ca values. This pattern can be observed in many interglacial periods either before or after the MBE (Figs. 6 and 7). MIS 31 presents one of the strongest SITIG gradients associated with a strong production and export of HSAC (high Sr/Ca values, Fig. 6). The U1467 Fe/K ratio record suggests very humid conditions in India during MIS 31, associated with low pelagic primary productivity (low Br) and a remarkable development of the carbonate factory (Fig. 6).

5.4 Implications for the Mid-Pleistocene transition and mid-Brunhes event

Together with the MPT, the MBE is considered a critical interval in the climate transitions of the Quaternary. During the MBE (ca. 430 ka) the large amplitude glacial–interglacial oscillations were established, giving rise to clear 100 kyr cycles, with severe glaciations and very warm interglacial optima that started with the MIS 12-11 climatic cycle (Jansen et al., 1986; Imbrie et al., 1993). However, some precursor events for the MBE have been described during MIS 13 and 14 (Barth et al., 2018; Ao et al., 2020). The CO_2 and temperature records from the Antarctic ice cores show a shift to warmer interglacial temperatures and higher CO_2 levels during the interglacial periods after the MBE (Bereiter et al., 2015; Jouzel et al., 2007), but the MBE is preceded by an interval of maximum $\delta^{13}C$ values during MIS 13 (Wang et al., 2003, 2014). In addition, around the MBE, the mid-Brunhes dissolution interval (MBDI) took place, with maximum dissolution centered at MIS 11 (Bassinot et al., 1994; Barker et al., 2006). The MBDI has been related to enhanced growth and calcification of the coccolithophores from the *Gephyrocapsa* complex (Rickaby et al., 2007; González-Lanchas et al., 2023) and enhanced carbonate production at platform tops (Droxler et al., 1990; Zeigler et al., 2003), which produced a change in the ocean's alkalinity and the shallowing of the carbonate compensation depth (Droxler et al., 1990; Hodell et al., 2001).

The Indian monsoon shows a clear shift towards more intense winter monsoon at the MPT, which is further enhanced at the MBE with stronger aridification during glacial periods (Kunkelova et al., 2018). This two-step pattern can be clearly observed in the CuSum plot of the Fe record (Fig. 8e), which shows a change at the MPT towards increasing dust input and a steeper gradient after the MBE (even higher glacial dust input). The increase in the winter monsoon strength during glacial periods drove changes in the ocean and atmospheric patterns of the Indian Ocean, including stronger aridification in India and higher dust input to the northern Indian Ocean (Kunkelova et al., 2018). In addition, changes in mid-depth ocean ventilation can be observed, which are related to the contraction of the oxygen minimum zone and the increase in the influence of the Antarctic Intermediate waters in the northern Indian Ocean (Alvarez Zarikian et al., 2022). Higher bottom water ventilation at the Maldives Inner Sea is observed during glacial periods starting at the MPT and ventilation further increased at the MBE (Alvarez Zarikian et al., 2022). This seafloor ventilation scenario is consistent with an intensification of the bioturbation patterns observed during interglacial periods (Reolid and Betzler, 2019). Other authors proposed a third step before the MBE (Ao et al., 2020), the intensification of the summer monsoon during MIS 13 due to the northward displacement of the ITCZ. This phenomenon created a temperature and precipitation asymmetry between hemispheres and a change in the global carbon cycle (Ao et al., 2020). The ITCZ displacement is also supported by the record of the Agulhas leakage fauna, which also started in MIS 13 to be frequent during interglacials, indicating a global change in ocean circulation during this interglacial period (Nuber et al., 2023). The interhemispheric asymmetry probably started with the MPT, when it has been hypothesized that the East Antarctic ice sheet (EAIS) margin grew out onto the shelf, driving further cooling in Antarctica and a stronger synchronicity between the waxing and waning of both hemispheres' ice sheets (Raymo et al., 2006). The climatic change in the MBE towards globally warmer conditions and higher sea level during MIS 11 is probably related to the partial melt of the Greenland and West Antarctic ice sheets (WAIS) as changes in the EAIS were relatively minor

(Raymo and Mitrovica, 2012) or limited to MIS 5, 9, and 11 (Wilson et al., 2018). MIS 11 may represent the initiation of interglacial periods in which both hemispheres were more symmetric.

In the U1467 record, particularly outstanding values of Sr/Ca occurred during MIS 11c, indicating a period in which a remarkable development of the shallow-marine carbonate factory occurred in the Maldives platform, depositing large amounts of Sr-rich carbonates. Similar high carbonate production has also been described for this time interval in other places such as the Great Barrier Reef, the Florida Keys, Belize reefs, and the Great Bahama Bank (Zeigler et al., 2003, and references therein). Moreover, it has been recently proposed that the modern tropical atolls, as we know them today, were established after the MBE (Droxler and Jorry, 2021). What precisely changed in the ocean to produce this change-over in the growing pattern of several carbonate platforms is still being debated. It is likely that ocean circulation shifts, such as the weakening of the Indonesian throughflow (Petrick et al., 2019) and the intensification of the Agulhas Current (Nuber et al., 2023), may have played an important role in modifying the monsoon system. This modification in the monsoon regime is also supported by the Mid-Pleistocene changes observed in the Australian monsoon (Gong et al., 2023). MIS 11 reconstructions (Figs. 4 and 8) indicate that sea level was probably the highest over the last 1 Myr (Elderfield et al., 2012; Spratt and Lisiecki, 2016; Miller et al., 2020). But more importantly, the sea-level rise occurred gradually during the longest termination of the last 1 Myr (Tzedakis et al., 2022), providing excellent conditions for carbonate factories to thrive within the Maldives Sea and on other carbonate platforms. Eustatic sea level during MIS 11 highstand (during the second half of MIS 11) has been estimated between 6 and 13 m above present sea level (Raymo and Mitrovica, 2012; Dutton et al., 2015). The sea-level records indicate that the eustatic rise was rather rapid during the termination, and after $\sim$ 419 ka sea-level increase slowed down and was punctuated by small sea-level falls (Fig. 8). It is likely that the ice sheets that disintegrated during MIS 11 (Greenland and WAIS) did not collapse at once but in several steps allowing for the growth of corals and other carbonate producers in the atolls. This argument would explain why HSAC production and export was high and pervasive during MIS 11 at the Maldives. The fact that sea-level rise was relatively gradual and that the SST and monsoonal conditions were optimal for carbonate platform producers triggered the greatest carbonate production and export rates within the Maldives record. MIS 11 represents a period of very high carbonate production and export, at least in the Maldives record, that without any doubt contributed to a change in the ocean's alkalinity during this interval.

However, the Maldives record shows that sea level is not the only factor conditioning high productivity and sediment export. The interval from MIS 29 to MIS 25 is characterized by the lowest Sr/Ca values among the interglacial periods, indicating unfavorable conditions for the development of the carbonate factories even though sea level was high. The CuSum plot for Sr/Ca (Fig. 8g) shows indeed a trend of decreasing carbonate production and export, particularly from MIS 31 to 22. Before the MPT, only MIS 31 and 35 show a good development of the carbonate factories, which coincides with periods of strong summer monsoon (high Fe/K ratio in Fig. 6), especially during MIS 31. Climatic records from MIS 31 show that this particularly long interglacial was characterized by warm and sustained SST (Medina-Elizalde and Lea, 2005; Weirauch et al., 2008; Herbert et al., 2010; Lawrence et al., 2010), with strong reductions in the Northern Hemisphere (NH) and West Antarctic ice sheets (Scherer et al., 2008; Melles et al., 2012). Moreover, MIS 31 is characterized by high SITIG and rather humid conditions on the continents, including strong summer monsoons (Sun et al., 2006; Girone et al., 2013; Grant et al., 2017; Oliveira et al., 2017; Justino et al., 2019). The high Sr/Ca values during MIS 31 coincides with high values in the Fe/K ratio, indicating that the strong summer monsoon boosted the development of the carbonate factory during this interglacial.

The Sr/Ca CuSum plot (Fig. 8g) shows a clear change at the MPT in the HSAC production and export, from a decreasing trend to a constant one, which suggests an increase and more constant development of the carbonate factory with respect to the previous interval. After the MBE, the conditions changed towards stronger development of the carbonate factory during interglacial maxima. Higher HSAC production in the low-latitude carbonate banks may be related to the sustained high sea level, warm SST of the interglacial maxima, and higher salinity developed in the western Indian Ocean due to a pervasive positive IOD. It can be noted that the high Sr/Ca values observed during MIS 5e, for example, follow the sea-level changes but also the dust input and the SITIG oscillations (Fig. 7), which may have stimulated the carbonate deposition at the reef environments in the Maldives Archipelago. Intense summer monsoon conditions have also been inferred for the Arabian Sea during MIS 13 (Ziegler et al., 2010). According to our data (Fig. 6), the enhanced carbonate platform development during MIS 13a and 17 was clearly favored by the intensification of the summer monsoon and positive IOD, although a sea-level threshold is also necessary for the establishment of carbonate producers in the atolls. Indeed, multiple sea-level reconstructions indicate that the sea-level difference between those interglacials before the MBE and the Holocene was rather low (Elderfield et al., 2012; Rohling et al., 2009; Spratt and Lisiecki, 2016). MIS 17 and 13a are characterized by slightly lower global SST and sea level, with respect to present (Medina-Elizalde and Lea, 2005; Herbert et al., 2010; Elderfield et al., 2012; PAGES-Past Interglacials Working Group, 2016; Spratt and Lisiecki, 2016; Rodrigues et al., 2017) but also by very humid conditions in southern Europe and the South Asian region (Sun et al., 2006; Sánchez Goñi et al., 2019; Oliveira et al., 2020). It has been hypothesized that the size of the

NH ice sheets was probably reduced as during other interglacial periods, but the West Antarctic ice sheet was slightly larger than during the interglacials after the MBE (Shi et al., 2020). This would explain the colder temperatures recorded in Antarctic ice cores (Jouzel et al., 2007) and the lower CO_2 values of the "lukewarm" interglacials compared the interglacial periods after the MBE (Bereiter et al., 2015). The slightly higher ice volume that accumulated in the West Antarctic ice sheet would have strengthened the asymmetry between the hemispheres, contributing to a northward shift in the ITCZ, stronger land–sea thermal contrast, and greater precipitation in South Asia during MIS 13 and probably MIS 17 (Shi et al., 2020). As a result, all the climatic belts would shift, including the Southern Hemisphere subpolar front, reported to have been in a northern position before the MBE, allowing the expansion of sea ice in the Southern Ocean and reducing the primary productivity in this location (Becquey and Gersonde, 2002; Martínez-Garcia et al., 2009; Jaccard et al., 2013).

Previously, it was suggested that slightly larger NH ice sheets would have also enhanced the East Asian monsoon through the intensification of a wave train that amplifies the Asian land–ocean summer pressure gradient (Yin et al., 2009). However, this explanation for more intense Asian summer monsoon does not apply for the Indian monsoon, which is weaker if the NH ice sheets are larger (Zhisheng et al., 2011). Furthermore, many high-latitude NH localities indicate a rather warm and humid climate during those interglacial periods, incompatible with larger NH ice sheets (Prokopenko et al., 2002; Wright and Flower, 2002; de Vernal and Hillaire-Marcel, 2008; Alonso-Garcia et al., 2011a; Melles et al., 2012; Hao et al., 2015; Lozhkin et al., 2017; Barker et al., 2019; Wang et al., 2023). In addition, MIS 14 stands out in the benthic $\delta^{18}O$ records as a moderate glacial period with short duration (e.g., Ahn et al., 2017) and higher sea level (Elderfield et al., 2012) than during other glacial periods (Fig. 8). The interval between MIS 15 and 13 shows very active formation of North Atlantic Deep Water (NADW) compared to other climatic cycles (Wright and Flower, 2002; Hodell et al., 2008; Alonso-Garcia et al., 2011b) and several records indicate that the rather humid and mild conditions of the interval between MIS 15 and 13 are related to the limited extent of Arctic ice sheets and the asymmetry between the ice sheets of the Northern and Southern Hemisphere (Hao et al., 2015; Candy and Alonso-Garcia, 2018; Ao et al., 2020). In the East Asian monsoon records, MIS 15–13 is a very interesting period with a weak winter monsoon and with an increasing trend in the summer monsoon proxy towards much wetter interglacial periods, MIS 13 being the first very humid interglacial period of the last 1 Myr (Ao et al., 2020; Ao et al., 2023). The Indian summer monsoon proxy (Fe/K ratio from U1467, Fig. 6) does not show the same transition towards very humid interglacials after MIS 13, but the interval MIS 15–13 was a rather humid period, indicating that glacial conditions were mild during MIS 14. MIS 13 stands out as a period with a strong development of the carbonate factory for a long interval (about 35 kyr), probably related to this change that affected the East Asian monsoon, enhancing the rainfall during the interglacial periods. The Indian summer monsoon and carbonate factory proxies from U1467 indicate that a shift in the ocean–atmosphere dynamics, probably related to a change in the Indonesian throughflow (Petrick et al., 2019), increased the intensity of the summer monsoon and favored positive IOD conditions, boosting the development of the carbonate producers in the atolls of the Maldives platform. The enhanced development of the carbonate factory also coincides with the establishment of the modern reefs (Droxler and Jorry, 2021). Further work needs to be done to unravel the exact factors that allowed this change at the MBE in the Maldives and other carbonate platforms.

6 Conclusions

High-resolution elemental geochemical records from IODP Site U1467, in the Maldives Inner Sea, have been examined in order to assess the factors controlling carbonate production and sediment export from the atolls to the basin. The Sr/Ca record indicates that most of the interglacial periods of the last 1.3 Myr presented an interval with high Sr-rich carbonate production and sediment export, which coincided with high sea level, regionally high SST, and strong Indian summer monsoon. The U1467 records indicate that sea level is an important factor in the development of the carbonate factory but temperature and monsoon dynamics also play a major role during interglacial periods.

Before the MBE ($\sim$ 430 ka), MIS 31, 17, and 13 stand out with high Sr/Ca values, although the highest Sr/Ca values of the last 1.3 Myr were attained during MIS 11. After the MBE, high Sr/Ca values are recorded at every interglacial optimum but they were particularly high during MIS 11, MIS 5, and the Holocene. MIS 31, well known as a rather warm interglacial, exhibits a remarkably high development of the carbonate factory that has been explained by the sustained strong Indian summer monsoon conditions, high SST, and high SITIG. The high Sr/Ca values observed during MIS 17 and 13 are more surprising since these periods have been considered lukewarm interglacials by some authors. The high-resolution elemental records of Site U1467 indicate that the Indian summer monsoon intensity and the Indian Ocean dipole dynamics may have played a significant role by reducing mixing of the upper water column (which in turn reduces turbidity) and maintaining the appropriate temperatures and salinities of sea-surface waters. Regardless of the sea-level conditions, the interglacial intervals between MIS 29 and 25 did not develop substantial carbonate production probably because the sea-surface conditions were not optimal (i.e., IOD was probably in a negative mode and summer monsoon conditions in India were not as strong as during other interglacials). The extremely high carbonate production

during MIS 11 was probably related to the gradual increase in sea level combined with pervasive strong Indian summer monsoon conditions and positive IOD. The extensive carbonate production and sediment export at the Maldives platforms contributed to a change in the global alkalinity and to increase the carbonate dissolution during the mid-Brunhes dissolution interval.

The cumulative sum analysis of the U1467 proxies for Indian summer and winter monsoon indicate a two-step increase in aridity (at the MPT and MBE) with enhanced dust input and mechanical weathering during glacial periods, probably driven by an increase in ice accumulation in both hemispheres during glacial periods. Moreover, the cumulative sum analysis of the U1467 Sr/Ca record suggests a decrease in the carbonate production and sediment export before the MPT, followed by a period with constant or moderate increase in the carbonate factory and an intensification in the carbonate production and sediment export at the MBE. Prior to MIS 11 only MIS 31, 17, and 13 showed a remarkable development of the carbonate factory in the Maldives atolls. We associate these intervals of high carbonate production with strong Indian summer monsoon conditions and positive IOD conditions coinciding with a sea-level optimum. After the MBE, all the interglacial periods seem to present more favorable conditions for carbonate production in the atolls, indicating a shift in the interglacial monsoonal conditions and in the oceanographic regime.

Data availability. The data displayed in this article is available at https://doi.org/10.5281/zenodo.8280041 (Alonso-Garcia et al., 2023).

Supplement. The supplement related to this article is available online at: https://doi.org/10.5194/cp-20-547-2024-supplement.

Author contributions. MAG, JR, FJJE, and OMB undertook conceptualization, design of the study, drawing of figures, and development of the first draft. MAG, CAAZ, OMB, JR, JCL, LJ, IC, JJGR, GPE, and CB were involved in performing the XRF analyses and/or funded the analyses. FJJE and MAG performed statistical analyses on the dataset. MAG, FJJE, JR, OMB, CAAZ, JCL, LJ, IC, JJGR, and CB contributed to the interpretation of the dataset and writing of the final version of the article.

Competing interests. The contact author has declared that none of the authors has any competing interests.

Special issue statement. This article is part of the special issue "Paleoclimate, from observing modern processes to reconstructing the past: a tribute to Dick (Dirk) Kroon". It is not associated with a conference.

Disclaimer. Publisher's note: Copernicus Publications remains neutral with regard to jurisdictional claims made in the text, published maps, institutional affiliations, or any other geographical representation in this paper. While Copernicus Publications makes every effort to include appropriate place names, the final responsibility lies with the authors.

Acknowledgements. We acknowledge IODP for providing the Expedition 359 sediment cores. The authors would like to acknowledge the reviewers (Jesse Farmer and Francisco J. Sierro) and editors for their very constructive comments that undoubtedly helped us to improve the article. We also would like to thank Dick Kroon for all his work and contributions to numerous paleoceanography studies, especially those regarding IODP Expedition 359. He was a wonderful human being and an enthusiastic and inspiring colleague that motivated and encouraged many people, and over time we all learned a lot from him.

Financial support. Montserrat Alonso-Garcia acknowledges funding from projects PICTURE (PID2021-128322NB-I00) and INDRA (EXPL/CTACLI/0612/2021). Luigi Jovane and Igor Carrasquiera are supported by Fundação de Amparo a Pesquisa no Estado de São Paulo (FAPESP) process 2016/24946-9. John J. G. Reijmer acknowledges funding from Vrije Universiteit Amsterdam MSc project fund. Carlos A. Alvarez Zarikian and Juan Carlos Laya acknowledge financial support from the US Science Support Program at Columbia University under post-expedition award no. OCE14-50528 and NSF award no. OCE-1326927.

Review statement. This paper was edited by Simon Jung and reviewed by Jesse Farmer and Francisco J. Sierro.

References

Abe-Ouchi, A., Saito, F., Kawamura, K., Raymo, M. E., Okuno, J. i., Takahashi, K., and Blatter, H.: Insolation-driven 100,000-year glacial cycles and hysteresis of ice-sheet volume, Nature, 500, 190–193, https://doi.org/10.1038/nature12374, 2013.

Ahn, S., Khider, D., Lisiecki, L. E., and Lawrence, C. E.: A probabilistic Pliocene–Pleistocene stack of benthic δ^{18}O using a profile hidden Markov model, Dynamics and Statistics of the Climate System, 2, dzx002, https://doi.org/10.1093/climsys/dzx002, 2017.

Aitchison, J.: The Statistical Analysis of Compositional Data, J. Roy. Stat. Soc. B Met., 44, 139–177, 1982.

Alonso-Garcia, M., Sierro, F. J., and Flores, J. A.: Arctic front shifts in the subpolar North Atlantic during the Mid-Pleistocene (800–400 ka) and their implications for ocean circulation, Palaeogeogr. Palaeocl., 311, 268–280, https://doi.org/10.1016/j.palaeo.2011.09.004, 2011a.

Alonso-Garcia, M., Sierro, F. J., Kucera, M., Flores, J. A., Cacho, I., and Andersen, N.: Ocean circulation, ice sheet growth and interhemispheric coupling of millennial climate variability during the mid-Pleistocene (ca 800–400 ka), Quaternary Sci. Rev.,

30, 3234–3247, https://doi.org/10.1016/j.quascirev.2011.08.005, 2011b.

Alonso-Garcia, M., Rodrigues, T., Abrantes, F., Padilha, M., Alvarez-Zarikian, C. A., Kunkelova, T., Wright, J. D., and Betzler, C.: Sea-surface temperature, productivity and hydrological changes in the Northern Indian Ocean (Maldives) during the interval ∼ 575–175 ka (MIS 14 to 7), Palaeogeogr. Palaeocl., 536, 109376, https://doi.org/10.1016/j.palaeo.2019.109376, 2019.

Alonso-Garcia, M., Reolid, J., Jimenez-Espejo, F. J., Bialik, O. M., Alvarez Zarikian, C. A., Laya, J. C., Carrasqueira, I., Jovane, L., Reijmer, J. J. G., Betzler, C., and Eberli, G. P.: Dataset: Sea-level and monsoonal control on the Maldives carbonate platform (Indian Ocean) over the last 1.3 million years [Data set], Zenodo [data set], https://doi.org/10.5281/zenodo.8280041, 2023.

Alvarez Zarikian, C. A., Nadiri, C., Alonso-García, M., Rodrigues, T., Huang, H.-H. M., Lindhorst, S., Kunkelova, T., Kroon, D., Betzler, C., and Yasuhara, M.: Ostracod response to monsoon and OMZ variability over the past 1.2 Myr, Mar. Micropaleontol., 174, 102105, https://doi.org/10.1016/j.marmicro.2022.102105, 2022.

Antoine, D., André, J.-M., and Morel, A.: Oceanic primary production: 2. Estimation at global scale from satellite (Coastal Zone Color Scanner) chlorophyll, Global Biogeochem. Cy., 10, 57–69, https://doi.org/10.1029/95GB02832, 1996.

Ao, H., Rohling, E. J., Stringer, C., Roberts, A. P., Dekkers, M. J., Dupont-Nivet, G., Yu, J., Liu, Q., Zhang, P., Liu, Z., Ma, X., Zhou, W., Jin, Z., Xiao, G., Wang, H., Sun, Q., Yang, P., Peng, X., Shi, Z., Qiang, X., and An, Z.: Two-stage mid-Brunhes climate transition and mid-Pleistocene human diversification, Earth-Sci. Rev., 210, 103354, https://doi.org/10.1016/j.earscirev.2020.103354, 2020.

Ao, H., Rohling, E. J., Li, X., Song, Y., Roberts, A. P., Han, Y., Poulsen, C. J., Jonell, T. N., Liebrand, D., Sun, Q., Li, X., Qiang, X., Zhang, P., and Dekkers, M. J.: Northern Hemisphere ice sheet expansion intensified Asian aridification and the winter monsoon across the mid-Pleistocene transition, Communications Earth & Environment, 4, 36, https://doi.org/10.1038/s43247-023-00686-9, 2023.

Aubert, O. and Droxler, A.: Seismic stratigraphy and depositional signatures of the Maldive carbonate system (Indian Ocean), Mar. Petrol. Geol., 13, 503–536, https://doi.org/10.1016/0264-8172(96)00008-6, 1996.

Barker, S., Archer, D., Booth, L., Elderfield, H., Henderiks, J., and Rickaby, R. E. M.: Globally increased pelagic carbonate production during the Mid-Brunhes dissolution interval and the CO_2 paradox of MIS 11, Quaternary Sci. Rev., 25, 3278–3293, 2006.

Barker, S., Knorr, G., Conn, S., Lordsmith, S., Newman, D., and Thornalley, D.: Early Interglacial Legacy of Deglacial Climate Instability, Paleoceanography and Paleoclimatology, 34, 1455–1475, https://doi.org/10.1029/2019pa003661, 2019.

Barth, A. M., Clark, P. U., Bill, N. S., He, F., and Pisias, N. G.: Climate evolution across the Mid-Brunhes Transition, Clim. Past, 14, 2071–2087, https://doi.org/10.5194/cp-14-2071-2018, 2018.

Bassinot, F. C., Beaufort, L., Vincent, E., Labeyrie, L. D., Rostek, F., Müller, P. J., Quidelleur, X., and Lancelot, Y.: Coarse Fraction Fluctuations in Pelagic Carbonate Sediments from the Tropical Indian Ocean: A 1500-Kyr Record of Carbonate Dissolution, Paleoceanography, 9, 579–600, https://doi.org/10.1029/94pa00860, 1994.

Beck, J. W., Zhou, W., Li, C., Wu, Z., White, L., Xian, F., Kong, X., and An, Z.: A 550,000-year record of East Asian monsoon rainfall from ^{10}Be in loess, Science, 360, 877–881, https://doi.org/10.1126/science.aam5825, 2018.

Becquey, S. and Gersonde, R.: Past hydrographic and climatic changes in the Subantarctic Zone of the South Atlantic – The Pleistocene record from ODP Site 1090, Palaeogeogr. Palaeocl., 182, 221–239, 2002.

Belopolsky, A. and Droxler, A.: Imaging Tertiary carbonate system—the Maldives, Indian Ocean : Insights into carbonate sequence interpretation, Leading Edge, 22, 646–652, https://doi.org/10.1190/1.1599690, 2003.

Bereiter, B., Eggleston, S., Schmitt, J., Nehrbass-Ahles, C., Stocker, T. F., Fischer, H., Kipfstuhl, S., and Chappellaz, J.: Revision of the EPICA Dome C CO_2 record from 800 to 600 kyr before present, Geophys. Res. Lett., 42, 542–549, https://doi.org/10.1002/2014gl061957, 2015.

Berger, A., Mélice, J. L., and Loutre, M. F.: On the origin of the 100-kyr cycles in the astronomical forcing, Paleoceanography, 20, PA4019, https://doi.org/10.1029/2005pa001173, 2005.

Betzler, C. and Eberli, G. P.: Miocene start of modern carbonate platforms, Geology, 47, 771–775, https://doi.org/10.1130/g45994.1, 2019.

Betzler, C., Hübscher, C., Lindhorst, S., Reijmer, J. J. G., Römer, M., Droxler, A. W., Fürstenau, J., and Lüdmann, T.: Monsoon-induced partial carbonate platform drowning (Maldives, Indian Ocean), Geology, 37, 867–870, https://doi.org/10.1130/g25702a.1, 2009.

Betzler, C., Lüdmann, T., Hübscher, C., and Fürstenau, J.: Current and sea-level signals in periplatform ooze (Neogene, Maldives, Indian Ocean), Sediment. Geol., 290, 126–137, https://doi.org/10.1016/j.sedgeo.2013.03.011, 2013.

Betzler, C., Eberli, G. P., Kroon, D., Wright, J. D., Swart, P. K., Nath, B. N., Alvarez-Zarikian, C. A., Alonso-García, M., Bialik, O. M., Blättler, C. L., Guo, J. A., Haffen, S., Horozal, S., Inoue, M., Jovane, L., Lanci, L., Laya, J. C., Ling, A. H. M., Lüdmann, T., Nakakuni, M., Niino, K., Petruny, L. M., Pratiwi, S. D., Reijmer, J. J. G., Reolid, J., Slagle, A. L., Sloss, C. R., Su, X., Yao, Z., and Young, J. R.: The abrupt onset of the modern South Asian Monsoon winds, Sci. Rep., 6, 29838, https://doi.org/10.1038/srep29838, 2016a.

Betzler, C. G., Eberli, G. P., Alvarez-Zarikian, C. A., Alonso-Garcia, M., Bialik, O. M., Blättler, C. L., Guo, J. A., Haffen, S., Horozal, S., Inoue, M., Jovane, L., Kroon, D., Lanci, L., Laya, J. C., Ling, A. H. M., Lüdmann, T., Nakakuni, M., Nath, B. N., Niino, K., Petruny, L. M., Pratiwi, S. D., Reijmer, J. J. G., Reolid, J., Slagle, A. L., Sloss, C., Su, X., Swart, P. K., Wright, J. D., Yao, Z., and Young, J. R.: Expedition 359 Preliminary Report: Maldives Monsoon and Sea Level, International Ocean Discovery Program, https://doi.org/10.14379/iodp.pr.359.2016, 2016b.

Betzler, C., Eberli, G. P., Alvarez Zarikian, C. A., Alonso-García, M., Bialik, O. M., Blättler, C. L., Guo, J. A., Haffen, S., Horozal, S., Inoue, M., Jovane, L., Kroon, D., Lanci, L., Laya, J. C., Ling Hui Mee, A., Lüdmann, T., Nakakuni, M., Nath, B. N., Niino, K., Petruny, L. M., Pratiwi, S. D., Reijmer, J. J. G., Reolid, J., Slagle, A. L., Sloss, C. R., Su, X., Swart, P. K., Wright, J. D., Yao, Z., and Young, J. R.: Maldives Monsoon and Sea Level, in: Proceedings of the International Ocean Discovery Program,

359, College Station, TX, International Ocean Discovery Program, https://doi.org/10.14379/iodp.proc.359.2017, 2017.

Betzler, C., Eberli, G. P., Lüdmann, T., Reolid, J., Kroon, D., Reijmer, J. J. G., Swart, P. K., Wright, J., Young, J. R., Alvarez-Zarikian, C., Alonso-García, M., Bialik, O. M., Blättler, C. L., Guo, J. A., Haffen, S., Horozal, S., Inoue, M., Jovane, L., Lanci, L., Laya, J. C., Hui Mee, A. L., Nakakuni, M., Nath, B. N., Niino, K., Petruny, L. M., Pratiwi, S. D., Slagle, A. L., Sloss, C. R., Su, X., and Yao, Z.: Refinement of Miocene sea level and monsoon events from the sedimentary archive of the Maldives (Indian Ocean), Progress in Earth and Planetary Science, 5, 5, https://doi.org/10.1186/s40645-018-0165-x, 2018.

Betzler, C. G., Eberli, G. P., Alvarez-Zarikian, C. A., Alonso-Garcia, M., Bejugam, N. N., Bialik, O. M., Blättler, C. L., Guo, J. A., Haffen, S., Horozal, S., Inoue, M., Jovane, L., Kroon, D., Lanci, L., Laya, J. C., Ling, A. H. M., Lüdmann, T., Nakakuni, M., Niino, K., Petruny, L. M., Pratiwi, S. D., Reijmer, J. J. G., Reolid, J., Slagle, A. L., Sloss, C., Su, X., Swart, P. K., Wright, J. D., Yao, Z., and Young, J. R.: Expedition 359 Preliminary Report: Maldives Monsoon and Sea Level, International Ocean Discovery Program, https://doi.org/10.14379/iodp.pr.359.2016, 2016.

Bialik, O. M., Reolid, J., Betzler, C., Eberli, G. P., and Waldmann, N. D.: Source shifts to periplatform deposits during the early to middle Miocene in response to climatic and oceanographic forcing, Maldives, western Indian Ocean, Palaeogeogr. Palaeocl., 559, 109969, https://doi.org/10.1016/j.palaeo.2020.109969, 2020.

Bialik, O. M., Sisma-Ventura, G., Vogt-Vincent, N., Silverman, J., and Katz, T.: Role of oceanic abiotic carbonate precipitation in future atmospheric CO_2 regulation, Sci. Rep.-UK, 12, 15970, https://doi.org/10.1038/s41598-022-20446-7, 2022.

Boardman, M. R., Neumann, A. C., Baker, P. A., Dulin, L. A., Kenter, R. J., Hunter, G. E., and Kiefer, K. B.: Banktop responses to Quaternary fluctuations in sea level recorded in periplatform sediments, Geology, 14, 28–31, https://doi.org/10.1130/0091-7613(1986)14<28:BRTQFI>2.0.CO;2, 1986.

Bosmans, J. H. C., Hilgen, F. J., Tuenter, E., and Lourens, L. J.: Obliquity forcing of low-latitude climate, Clim. Past, 11, 1335–1346, https://doi.org/10.5194/cp-11-1335-2015, 2015.

Bunzel, D., Schmiedl, G., Lindhorst, S., Mackensen, A., Reolid, J., Romahn, S., and Betzler, C.: A multi-proxy analysis of Late Quaternary ocean and climate variability for the Maldives, Inner Sea, Clim. Past, 13, 1791–1813, https://doi.org/10.5194/cp-13-1791-2017, 2017.

Cai, W., Wang, G., Li, Z., Zheng, X., Yang, K., and Ng, B.: Chapter 21 – Response of the positive Indian Ocean dipole to climate change and impact on Indian summer monsoon rainfall, in: Indian Summer Monsoon Variability, edited by: Chowdary, J., Parekh, A., and Gnanaseelan, C., Elsevier, https://doi.org/10.1016/B978-0-12-822402-1.00010-7, 413–432, 2021.

Cai, Y., Zhang, H., Cheng, H., An, Z., Lawrence Edwards, R., Wang, X., Tan, L., Liang, F., Wang, J., and Kelly, M.: The Holocene Indian monsoon variability over the southern Tibetan Plateau and its teleconnections, Earth Planet. Sc. Lett., 335–336, 135–144, https://doi.org/10.1016/j.epsl.2012.04.035, 2012.

Caley, T., Extier, T., Collins, J. A., Schefuß, E., Dupont, L., Malaizé, B., Rossignol, L., Souron, A., McClymont, E. L., Jimenez-Espejo, F. J., García-Comas, C., Eynaud, F., Martinez, P., Roche, D. M., Jorry, S. J., Charlier, K., Wary, M., Gourves, P.-Y., Billy, I., and Giraudeau, J.: A two-million-year-long hydroclimatic context for hominin evolution in southeastern Africa, Nature, 560, 76–79, https://doi.org/10.1038/s41586-018-0309-6, 2018.

Candy, I. and Alonso-Garcia, M.: A 1 Ma sea surface temperature record from the North Atlantic and its implications for the early human occupation of Britain, Quaternary Res., 90, 406–417, https://doi.org/10.1017/qua.2018.62, 2018.

Candy, I. and McClymont, E. L.: Interglacial intensity in the North Atlantic over the last 800 000 years: investigating the complexity of the mid-Brunhes Event, J. Quaternary Sci., 28, 343–348, https://doi.org/10.1002/jqs.2632, 2013.

Candy, I., Schreve, D. C., Sherriff, J., and Tye, G. J.: Marine Isotope Stage 11: Palaeoclimates, palaeoenvironments and its role as an analogue for the current interglacial, Earth-Sci. Rev., 128, 18–51, https://doi.org/10.1016/j.earscirev.2013.09.006, 2014.

Carrasqueira, I. G. D. F., Jovane, L., Droxler, A. W., Alvarez Zarikian, C. A., Lanci, L., Alonso-Garcia, M., Laya, J. C., and Kroon, D.: Anomalous widespread arid events in Asia over the past 550,000 years, PNAS Nexus, 2, 1–9, https://doi.org/10.1093/pnasnexus/pgad175, 2023.

Chalk, T. B., Hain, M. P., Foster, G. L., Rohling, E. J., Sexton, P. F., Badger, M. P. S., Cherry, S. G., Hasenfratz, A. P., Haug, G. H., Jaccard, S. L., Martínez-García, A., Pälike, H., Pancost, R. D., and Wilson, P. A.: Causes of ice age intensification across the Mid-Pleistocene Transition, P. Natl. Acad. Sci. USA, 114, 13114–13119, https://doi.org/10.1073/pnas.1702143114, 2017.

Cheng, H., Edwards, R. L., Sinha, A., Spötl, C., Yi, L., Chen, S., Kelly, M., Kathayat, G., Wang, X., Li, X., Kong, X., Wang, Y., Ning, Y., and Zhang, H.: The Asian monsoon over the past 640,000 years and ice age terminations, Nature, 534, 640–646, https://doi.org/10.1038/nature18591, 2016.

Clark, P. U., Archer, D., Pollard, D., Blum, J. D., Rial, J. A., Brovkin, V., Mix, A. C., Pisias, N. G., and Roy, M.: The middle Pleistocene transition: characteristics, mechanisms, and implications for long-term changes in atmospheric pCO_2, Quaternary Sci. Rev., 25, 3150–3184, 2006.

Davis, R. and Ashton, N.: Landscapes, environments and societies: The development of culture in Lower Palaeolithic Europe, J. Anthropol. Archaeol., 56, 101107, https://doi.org/10.1016/j.jaa.2019.101107, 2019.

de Vernal, A. and Hillaire-Marcel, C.: Natural Variability of Greenland Climate, Vegetation, and Ice Volume During the Past Million Years, Science, 320, 1622–1625, https://doi.org/10.1126/science.1153929, 2008.

Drever, J. I.: The geochemistry of natural waters, in: Vol. 437, Englewood Cliffs, Prentice Hall, ISBN 10:0133513963, 1988.

Droxler, A., Haddad, G. A., Mucciarone, D., and Cullen, J.: Pliocene–Pleistocene Aragonite Cyclic Variations in Holes 714A and 716B (the Maldives) Compared with Hole 633A (the Bahamas): Records of Climate-Induced $CaCO_3$ Preservation at Intermediate Water Depths, Proc. scientific results, ODP, Leg 115, Mascarene Plateau, 539–577, https://doi.org/10.2973/odp.proc.sr.115.179.1990, 1990.

Droxler, A. W. and Jorry, S. J.: The Origin of Modern Atolls: Challenging Darwin's Deeply Ingrained Theory, Annu. Rev. Mar. Sci., 13, 537–573, https://doi.org/10.1146/annurev-marine-122414-034137, 2021.

Droxler, A. W., Schlager, W., and Whallon, C. C.: Quaternary aragonite cycles and oxygen-isotope record in Bahamian carbonate ooze, Geology, 11, 235–239, https://doi.org/10.1130/0091-7613(1983)11<235:QACAOR>2.0.CO;2, 1983.

Droxler, A. W., Morse, J. W., and Kornicker, W. A.: Controls on carbonate mineral accumulation in Bahamian basins and adjacent Atlantic Ocean sediments, J. Sediment. Res., 58, 120–130, https://doi.org/10.1306/212F8D2D-2B24-11D7-8648000102C1865D, 1988.

Duncan, R. A. and Hargreaves, R. B.,: $^{40}Ar/^{39}Ar$ geochronology of basement rocks from the Mascarene plateau, the Chagos Bank, and the Maldives Ridge. Proceedings Ocean Drilling Programme, Scientific Results, 115, 43–51, 1990.

Dutton, A., Carlson, A. E., Long, A. J., Milne, G. A., Clark, P. U., DeConto, R., Horton, B. P., Rahmstorf, S., and Raymo, M. E.: Sea-level rise due to polar ice-sheet mass loss during past warm periods, Science, 349, aaa4019, https://doi.org/10.1126/science.aaa4019, 2015.

Elderfield, H., Ferretti, P., Greaves, M., Crowhurst, S., McCave, I. N., Hodell, D., and Piotrowski, A. M.: Evolution of Ocean Temperature and Ice Volume Through the Mid-Pleistocene Climate Transition, Science, 337, 704–709, https://doi.org/10.1126/science.1221294, 2012.

Flores, J.-A., Marino, M., Sierro, F. J., Hodell, D. A., and Charles, C. D.: Calcareous plankton dissolution pattern and coccolithophore assemblages during the last 600 kyr at ODP Site 1089 (Cape Basin, South Atlantic): paleoceanographic implications, Palaeogeogr. Palaeocl., 196, 409–426, 2003.

Gadgil, S.: The Indian Monsoon And Its Variability, Annu. Rev. Earth Pl. Sc., 31, 429–467, https://doi.org/10.1146/annurev.earth.31.100901.141251, 2003.

Gadgil, S.: The monsoon system: Land–sea breeze or the ITCZ?, J. Earth Syst. Sci., 127, 1, https://doi.org/10.1007/s12040-017-0916-x, 2018.

Galway-Witham, J., Cole, J., and Stringer, C.: Aspects of human physical and behavioural evolution during the last 1 million years, J. Quaternary Sci., 34, 355–378, https://doi.org/10.1002/jqs.3137, 2019.

García-Comas, C., Stemmann, L., Ibanez, F., Berline, L., Mazzocchi, M. G., Gasparini, S., Picheral, M., and Gorsky, G.: Zooplankton long-term changes in the NW Mediterranean Sea: Decadal periodicity forced by winter hydrographic conditions related to large-scale atmospheric changes?, J. Marine Syst., 87, 216–226, https://doi.org/10.1016/j.jmarsys.2011.04.003, 2011.

Gildor, H. and Tziperman, E.: A sea ice climate switch mechanism for the 100-kyr glacial cycles, J. Geophys. Res., 106, 9117–9133, https://doi.org/10.1029/1999jc000120, 2001.

Girone, A., Capotondi, L., Ciaranfi, N., Di Leo, P., Lirer, F., Maiorano, P., Marino, M., Pelosi, N., and Pulice, I.: Paleoenvironmental changes at the lower Pleistocene Montalbano Jonico section (southern Italy): Global versus regional signals, Palaeogeogr. Palaeocl., 371, 62–79, https://doi.org/10.1016/j.palaeo.2012.12.017, 2013.

Gischler, E., Storz, D., and Schmitt, D.: Sizes, shapes, and patterns of coral reefs in the Maldives, Indian Ocean: the influence of wind, storms, and precipitation on a major tropical carbonate platform, Carbonate. Evaporite., 29, 73–87, https://doi.org/10.1007/s13146-013-0176-z, 2014.

Gong, L., Holbourn, A., Kuhnt, W., Opdyke, B., Zhang, Y., Ravelo, A. C., Zhang, P., Xu, J., Matsuzaki, K., Aiello, I., Beil, S., and Andersen, N.: Middle Pleistocene reorganization of Australian Monsoon, Nat. Commun., 14, 2002, https://doi.org/10.1038/s41467-023-37639-x, 2023.

González-Lanchas, A., Rickaby, R. E. M., Sierro, F. J., Rigual-Hernández, A. S., Alonso-García, M., and Flores, J. A.: Globally enhanced calcification across the coccolithophore Gephyrocapsa complex during the mid-Brunhes interval, Quaternary Sci. Rev., 321, 108375, https://doi.org/10.1016/j.quascirev.2023.108375, 2023.

Govin, A., Holzwarth, U., Heslop, D., Ford Keeling, L., Zabel, M., Mulitza, S., Collins, J. A., and Chiessi, C. M.: Distribution of major elements in Atlantic surface sediments (36° N–49° S): Imprint of terrigenous input and continental weathering, Geochem. Geophy. Geosy., 13, Q01013, https://doi.org/10.1029/2011GC003785, 2012.

Grant, K. M., Rohling, E. J., Westerhold, T., Zabel, M., Heslop, D., Konijnendijk, T., and Lourens, L.: A 3 million year index for North African humidity/aridity and the implication of potential pan-African Humid periods, Quaternary Sci. Rev., 171, 100–118, https://doi.org/10.1016/j.quascirev.2017.07.005, 2017.

Gupta, A. K., Sarkar, S., De, S., Clemens, S. C., and Velu, A.: Mid-Brunhes strengthening of the Indian Ocean Dipole caused increased equatorial East African and decreased Australasian rainfall, Geophys. Res. Lett., 37, L06706, https://doi.org/10.1029/2009gl042225, 2010.

Hallock, P.: Global change and modern coral reefs: New opportunities to understand shallow-water carbonate depositional processes, Sediment. Geol., 175, 19–33, https://doi.org/10.1016/j.sedgeo.2004.12.027, 2005.

Hallock, P. and Schlager, W.: Nutrient Excess and the Demise of Coral Reefs and Carbonate Platforms, Palaios, 1, 389–398, https://doi.org/10.2307/3514476, 1986.

Hammer, Ø., Harper, D. A. T., and Ryan, P. D.: PAST: Paleontological statistics software package for education and data analysis, Palaeontol. Electron., 4, 4, 2001.

Hao, Q., Wang, L., Oldfield, F., and Guo, Z.: Extra-long interglacial in Northern Hemisphere during MISs 15-13 arising from limited extent of Arctic ice sheets in glacial MIS 14, Sci. Rep.-UK, 5, 12103, https://doi.org/10.1038/srep12103, 2015.

Hastenrath, S., Nicklis, A., and Greischar, L.: Atmospheric-hydrospheric mechanisms of climate anomalies in the western equatorial Indian Ocean, J. Geophys. Res.-Oceans, 98, 20219–20235, https://doi.org/10.1029/93JC02330, 1993.

Hearty, P. J., Kindler, P., Cheng, H., and Edwards, R. L.: A +20 m middle Pleistocene sea-level highstand (Bermuda and the Bahamas) due to partial collapse of Antarctic ice, Geology, 27, 375–378, https://doi.org/10.1130/0091-7613(1999)027<0375:AMMPSL>2.3.CO;2, 1999.

Hedges, J. I. and Keil, R. G.: Sedimentary organic matter preservation: an assessment and speculative synthesis, Mar. Chem., 49, 81–115, https://doi.org/10.1016/0304-4203(95)00008-F, 1995.

Herbert, T. D., Peterson, L. C., Lawrence, K. T., and Liu, Z.: Tropical Ocean Temperatures Over the Past 3.5 Million Years, Science, 328, 1530–1534, https://doi.org/10.1126/science.1185435, 2010.

Hobart, B., Lisiecki, L. E., Rand, D., Lee, T., and Lawrence, C. E.: Late Pleistocene 100-kyr glacial cycles paced by preces-

sion forcing of summer insolation, Nat. Geosci., 16, 717–722, https://doi.org/10.1038/s41561-023-01235-x, 2023.

Hodell, D. A. and Channell, J. E. T.: Mode transitions in Northern Hemisphere glaciation: co-evolution of millennial and orbital variability in Quaternary climate, Clim. Past, 12, 1805–1828, https://doi.org/10.5194/cp-12-1805-2016, 2016.

Hodell, D. A., Charles, C. D., and Sierro, F. J.: Late Pleistocene evolution of the ocean's carbonate system, Earth Planet. Sc. Lett., 192, 109–124, 2001.

Hodell, D. A., Kanfoush, S. L., Venz, K. A., Charles, C. D., and Sierro, F. J.: The Mid-Brunhes Transition in ODP Sites 1089 and 1090 (Subantarctic South Atlantic), in: Earth's Climate and Orbital Eccentricity: The Marine Isotope Stage 11 Question, Geophysical Monograph 137, edited by: Droxler, A. W., Poore, R. Z., and Burckle, L. H., American Geophysical Union, Washington, 113–129, 2003.

Hodell, D. A., Channell, J. E. T., Curtis, J. H., Romero, O. E., and Röhl, U.: Onset of "Hudson Strait" Heinrich events in the eastern North Atlantic at the end of the middle Pleistocene transition (~ 640 ka)?, Paleoceanography, 23, PA4218, https://doi.org/10.1029/2008PA001591, 2008.

Honisch, B., Hemming, N. G., Archer, D., Siddall, M., and McManus, J. F.: Atmospheric Carbon Dioxide Concentration Across the Mid-Pleistocene Transition, Science, 324, 1551–1554, https://doi.org/10.1126/science.1171477, 2009.

Hormann, V., Centurioni, L. R., and Gordon, A. L.: Freshwater export pathways from the Bay of Bengal, Deep-Sea Res. Pt. II, 168, 104645, https://doi.org/10.1016/j.dsr2.2019.104645, 2019.

Huybers, P. and Wunsch, C.: Obliquity pacing of the late Pleistocene glacial terminations, Nature, 434, 491–494, 2005.

Ibanez, F., Fromentin, J., and Castel, J.: Application of the cumulated function to the processing of chronological data in oceanography, C. R. Acad. Sci. III-Vie., 316, 745–748, 1993.

Imbrie, J., Berger, A., Boyle, E. A., Clemens, S. C., Duffy, A., Howard, W. R., Kukla, G., Kutzbach, J., Martinson, D. G., McIntyre, A., Mix, A. C., Molfino, B., Morley, J. J., Peterson, L. C., Pisias, N. G., Prell, W. L., Raymo, M. E., Shackleton, N. J., and Toggweiler, J. R.: On the Structure and Origin of Major Glaciation Cycles 2. The 100,000-Year Cycle, Paleoceanography, 8, 699–735, https://doi.org/10.1029/93pa02751, 1993.

Inness, A., Ades, M., Agustí-Panareda, A., Barré, J., Benedictow, A., Blechschmidt, A.-M., Dominguez, J. J., Engelen, R., Eskes, H., Flemming, J., Huijnen, V., Jones, L., Kipling, Z., Massart, S., Parrington, M., Peuch, V.-H., Razinger, M., Remy, S., Schulz, M., and Suttie, M.: The CAMS reanalysis of atmospheric composition, Atmos. Chem. Phys., 19, 3515–3556, https://doi.org/10.5194/acp-19-3515-2019, 2019.

Jaccard, S. L., Hayes, C. T., Martínez-García, A., Hodell, D. A., Anderson, R. F., Sigman, D. M., and Haug, G. H.: Two Modes of Change in Southern Ocean Productivity Over the Past Million Years, Science, 339, 1419–1423, https://doi.org/10.1126/science.1227545, 2013.

Jansen, J. H. F., Kuijpers, A., and Troelstra, S. R.: A Mid-Brunhes Climatic Event: Long-Term Changes in Global Atmosphere and Ocean Circulation, Science, 232, 619–622, https://doi.org/10.1126/science.232.4750.619, 1986.

Jouzel, J., Masson-Delmotte, V., Cattani, O., Dreyfus, G., Falourd, S., Hoffmann, G., Minster, B., Nouet, J., Barnola, J. M., Chappellaz, J., Fischer, H., Gallet, J. C., Johnsen, S., Leuenberger, M., Loulergue, L., Luethi, D., Oerter, H., Parrenin, F., Raisbeck, G., Raynaud, D., Schilt, A., Schwander, J., Selmo, E., Souchez, R., Spahni, R., Stauffer, B., Steffensen, J. P., Stenni, B., Stocker, T. F., Tison, J. L., Werner, M., and Wolff, E. W.: Orbital and Millennial Antarctic Climate Variability over the Past 800,000 Years, Science, 317, 793–796, https://doi.org/10.1126/science.1141038, 2007.

Justino, F., Kucharski, F., Lindemann, D., Wilson, A., and Stordal, F.: A modified seasonal cycle during MIS31 super-interglacial favors stronger interannual ENSO and monsoon variability, Clim. Past, 15, 735–749, https://doi.org/10.5194/cp-15-735-2019, 2019.

Kench, P. S., McLean, R. F., and Nichol, S. L.: New model of reef-island evolution: Maldives, Indian Ocean, Geology, 33, 145–148, https://doi.org/10.1130/G21066.1, 2005.

Kench, P. S., Smithers, S. G., McLean, R. F., and Nichol, S. L.: Holocene reef growth in the Maldives: Evidence of a mid-Holocene sea-level highstand in the central Indian Ocean, Geology, 37, 455–458, https://doi.org/10.1130/G25590A.1, 2009.

Kench, P. S., Beetham, E. P., Turner, T., Morgan, K. M., Owen, S. D., and McLean, R. F.: Sustained coral reef growth in the critical wave dissipation zone of a Maldivian atoll, Communications Earth & Environment, 3, 9, https://doi.org/10.1038/s43247-021-00338-w, 2022.

Kennedy, M. J., Löhr, S. C., Fraser, S. A., and Baruch, E. T.: Direct evidence for organic carbon preservation as clay-organic nanocomposites in a Devonian black shale; from deposition to diagenesis, Earth Planet. Sc. Lett., 388, 59–70, https://doi.org/10.1016/j.epsl.2013.11.044, 2014.

Kolla, V., Kostecki, J. A., Robinson, F., Biscaye, P. E., and Ray, P. K.: Distributions and origins of clay minerals and quartz in surface sediments of the Arabian Sea, J. Sediment. Res., 51, 563–569, https://doi.org/10.1306/212F7CD9-2B24-11D7-8648000102C1865D, 1981.

Konijnendijk, T. Y. M., Ziegler, M., and Lourens, L. J.: On the timing and forcing mechanisms of late Pleistocene glacial terminations: Insights from a new high-resolution benthic stable oxygen isotope record of the eastern Mediterranean, Quaternary Sci. Rev., 129, 308–320, https://doi.org/10.1016/j.quascirev.2015.10.005, 2015.

Kotov, S. and Pälike, H.: QAnalySeries – a cross-platform time series tuning and analysis tool, AGU Fall Meeting Abstracts, vol. 2018, 10–14 December 2018, Washington, D.C., PP53D-1230, https://doi.org/10.1002/essoar.10500226.1, 2018.

Kunkelova, T., Jung, S. J. A., de Leau, E. S., Odling, N., Thomas, A. L., Betzler, C., Eberli, G. P., Alvarez-Zarikian, C. A., Alonso-García, M., Bialik, O. M., Blättler, C. L., Guo, J. A., Haffen, S., Horozal, S., Mee, A. L. H., Inoue, M., Jovane, L., Lanci, L., Laya, J. C., Lüdmann, T., Bejugam, N. N., Nakakuni, M., Niino, K., Petruny, L. M., Pratiwi, S. D., Reijmer, J. J. G., Reolid, J., Slagle, A. L., Sloss, C. R., Su, X., Swart, P. K., Wright, J. D., Yao, Z., Young, J. R., Lindhorst, S., Stainbank, S., Rueggeberg, A., Spezzaferri, S., Carrasqueira, I., Hu, S., and Kroon, D.: A two million year record of low-latitude aridity linked to continental weathering from the Maldives, Progress in Earth and Planetary Science, 5, 86, https://doi.org/10.1186/s40645-018-0238-x, 2018.

Kunkelova, T., Crocker, A. J., Jewell, A. M., Breeze, P. S., Drake, N. A., Cooper, M. J., Milton, J. A., Hennen, M.,

Shahgedanova, M., Petraglia, M., and Wilson, P. A.: Dust sources in Westernmost Asia have a different geochemical fingerprint to those in the Sahara, Quaternary Sci. Rev., 294, 107717, https://doi.org/10.1016/j.quascirev.2022.107717, 2022.

Lang, N. and Wolff, E. W.: Interglacial and glacial variability from the last 800 ka in marine, ice and terrestrial archives, Clim. Past, 7, 361–380, https://doi.org/10.5194/cp-7-361-2011, 2011.

Laskar, J., Robutel, P., Joutel, F., Gastineau, M., Correia, A. C. M., and Levrard, B.: A long-term numerical solution for the insolation quantities of the Earth, Astron. Astrophys., 428, 261–285, https://doi.org/10.1051/0004-6361:20041335, 2004.

Lawrence, K. T., Sosdian, S., White, H. E., and Rosenthal, Y.: North Atlantic climate evolution through the Plio-Pleistocene climate transitions, Earth Planet. Sc. Lett., 300, 329–342, https://doi.org/10.1016/j.epsl.2010.10.013, 2010.

Lebrato, M., Garbe-Schönberg, D., Müller, M. N., Blanco-Ameijeiras, S., Feely, R. A., Lorenzoni, L., Molinero, J.-C., Bremer, K., Jones, D. O. B., Iglesias-Rodriguez, D., Greeley, D., Lamare, M. D., Paulmier, A., Graco, M., Cartes, J., Barcelos e Ramos, J., de Lara, A., Sanchez-Leal, R., Jimenez, P., Paparazzo, F. E., Hartman, S. E., Westernströer, U., Küter, M., Benavides, R., da Silva, A. F., Bell, S., Payne, C., Olafsdottir, S., Robinson, K., Jantunen, L. M., Korablev, A., Webster, R. J., Jones, E. M., Gilg, O., Bailly du Bois, P., Beldowski, J., Ashjian, C., Yahia, N. D., Twining, B., Chen, X.-G., Tseng, L.-C., Hwang, J.-S., Dahms, H.-U., and Oschlies, A.: Global variability in seawater Mg : Ca and Sr : Ca ratios in the modern ocean, P. Natl. Acad. Sci. USA, 117, 22281–22292, https://doi.org/10.1073/pnas.1918943117, 2020.

Lindhorst, S., Betzler, C., and Kroon, D.: Wind variability over the northern Indian Ocean during the past 4 million years – Insights from coarse aeolian dust (IODP exp. 359, site U1467, Maldives), Palaeogeogr. Palaeocl., 536, 109371, https://doi.org/10.1016/j.palaeo.2019.109371, 2019.

Ling, A., Eberli, G. P., Swart, P. K., Reolid, J., Stainbank, S., Rüggeberg, A., and Betzler, C.: Middle Miocene platform drowning in the Maldives associated with monsoon-related intensification of currents, Palaeogeogr. Palaeocl., 567, 110275, https://doi.org/10.1016/j.palaeo.2021.110275, 2021.

Lisiecki, L. E.: Links between eccentricity forcing and the 100,000-year glacial cycle, Nat. Geosci., 3, 349–352, http://www.nature.com/ngeo/journal/v3/n5/suppinfo/ngeo828_S1.html, 2010.

Lozhkin, A. V., Minyuk, P. S., Anderson, P. M., Nedorubova, E. Y., and Korzun, J. V.: Variability in landscape and lake system responses to glacial and interglacial climates during the Middle Pleistocene based on palynological and geochemical data from Lake El'gygytgyn, Eastern Arctic, Rev. Palaeobot. Palyno., 246, 1–13, https://doi.org/10.1016/j.revpalbo.2017.06.004, 2017.

Lyle, M. and Backman, J.: Data report: calibration of XRF-estimated $CaCO_3$ along the Site U1338 splice, in: Pälike, H., Lyle, M., Nishi, H., Raffi, I., Gamage, K., Klaus, A., and the Expedition 320/321 Scientists, Proc. IODP, 320/321: Tokyo, Integrated Ocean Drilling Program Management International, Inc., https://doi.org/10.2204/iodp.proc.320321.205.2013, 2013.

Maher, B. A., Prospero, J. M., Mackie, D., Gaiero, D., Hesse, P. P., and Balkanski, Y.: Global connections between aeolian dust, climate and ocean biogeochemistry at the present day and at the last glacial maximum, Earth-Sci. Rev., 99, 61–97, https://doi.org/10.1016/j.earscirev.2009.12.001, 2010.

Mantsis, D. F., Lintner, B. R., Broccoli, A. J., Erb, M. P., Clement, A. C., and Park, H.-S.: The Response of Large-Scale Circulation to Obliquity-Induced Changes in Meridional Heating Gradients, J. Climate, 27, 5504–5516, https://doi.org/10.1175/jcli-d-13-00526.1, 2014.

Marchant, R., Mumbi, C., Behera, S., and Yamagata, T.: The Indian Ocean dipole – the unsung driver of climatic variability in East Africa, Afr. J. Ecol., 45, 4–16, https://doi.org/10.1111/j.1365-2028.2006.00707.x, 2007.

Martínez-Garcia, A., Rosell-Melé, A., Geibert, W., Gersonde, R., Masqué, P., Gaspari, V., and Barbante, C.: Links between iron supply, marine productivity, sea surface temperature, and CO_2 over the last 1.1 Ma, Paleoceanography, 24, PA1207, https://doi.org/10.1029/2008PA001657, 2009.

McClymont, E. L., Sosdian, S. M., Rosell-Melé, A., and Rosenthal, Y.: Pleistocene sea-surface temperature evolution: Early cooling, delayed glacial intensification, and implications for the mid-Pleistocene climate transition, Earth-Sci. Rev., 123, 173–193, https://doi.org/10.1016/j.earscirev.2013.04.006, 2013.

Medina-Elizalde, M. and Lea, D. W.: The Mid-Pleistocene Transition in the Tropical Pacific, Science, 310, 1009–1012, https://doi.org/10.1126/science.1115933, 2005.

Melles, M., Brigham-Grette, J., Minyuk, P. S., Nowaczyk, N. R., Wennrich, V., DeConto, R. M., Anderson, P. M., Andreev, A. A., Coletti, A., Cook, T. L., Haltia-Hovi, E., Kukkonen, M., Lozhkin, A. V., Rosén, P., Tarasov, P., Vogel, H., and Wagner, B.: 2.8 Million Years of Arctic Climate Change from Lake El'gygytgyn, NE Russia, Science, 337, 315–320, https://doi.org/10.1126/science.1222135, 2012.

Miller, K. G., Browning, J. V., Schmelz, W. J., Kopp, R. E., Mountain, G. S., and Wright, J. D.: Cenozoic sea-level and cryospheric evolution from deep-sea geochemical and continental margin records, Sci. Adv., 6, eaaz1346, https://doi.org/10.1126/sciadv.aaz1346, 2020.

Moncel, M.-H., Ashton, N., Lamotte, A., Tuffreau, A., Cliquet, D., and Despriée, J.: The Early Acheulian of northwestern Europe, J. Anthropol. Archaeol., 40, 302–331, https://doi.org/10.1016/j.jaa.2015.09.005, 2015.

Moncel, M.-H., Ashton, N., Arzarello, M., Fontana, F., Lamotte, A., Scott, B., Muttillo, B., Berruti, G., Nenzioni, G., Tuffreau, A., and Peretto, C.: Early Levallois core technology between Marine Isotope Stage 12 and 9 in Western Europe, J. Hum. Evol., 139, 102735, https://doi.org/10.1016/j.jhevol.2019.102735, 2020.

Mudelsee, M. and Schulz, M.: The Mid-Pleistocene climate transition: onset of 100 ka cycle lags ice volume build-up by 280 ka, Earth Planet. Sc. Lett., 151, 117–123, 1997.

Nuber, S., Rae, J. W. B., Zhang, X., Andersen, M. B., Dumont, M. D., Mithan, H. T., Sun, Y., de Boer, B., Hall, I. R., and Barker, S.: Indian Ocean salinity build-up primes deglacial ocean circulation recovery, Nature, 617, 306–311, https://doi.org/10.1038/s41586-023-05866-3, 2023.

Oliveira, D., Sánchez Goñi, M. F., Naughton, F., Polanco-Martínez, J. M., Jimenez-Espejo, F. J., Grimalt, J. O., Martrat, B., Voelker, A. H. L., Trigo, R., Hodell, D., Abrantes, F., and Desprat, S.: Unexpected weak seasonal climate in the western Mediterranean region during MIS 31, a high-insolation forced interglacial, Quaternary Sci. Rev., 161, 1–17, https://doi.org/10.1016/j.quascirev.2017.02.013, 2017.

Oliveira, D., Desprat, S., Yin, Q., Rodrigues, T., Naughton, F., Trigo, R. M., Su, Q., Grimalt, J. O., Alonso-Garcia, M., Voelker, A. H. L., Abrantes, F., and Sánchez Goñi, M. F.: Combination of insolation and ice-sheet forcing drive enhanced humidity in northern subtropical regions during MIS 13, Quaternary Sci. Rev., 247, 106573, https://doi.org/10.1016/j.quascirev.2020.106573, 2020.

Olson, S. L. and Hearty, P. J.: A sustained +21 m sea-level highstand during MIS 11 (400 ka): direct fossil and sedimentary evidence from Bermuda, Quaternary Sci. Rev., 28, 271–285, https://doi.org/10.1016/j.quascirev.2008.11.001, 2009.

Ota, Y., Kawahata, H., Kuroda, J., Suzuki, A., Abe-Ouchi, A., and Jimenez-Espejo, F. J.: Millennial-scale variability of Indian summer monsoon constrained by the western Bay of Bengal sediments: Implication from geochemical proxies of sea surface salinity and river runoff, Global Planet. Change, 208, 103719, https://doi.org/10.1016/j.gloplacha.2021.103719, 2022.

Page, E. S.: Continuous Inspection Schemes, Biometrika, 41, 100–115, https://doi.org/10.2307/2333009, 1954.

PAGES – Past Interglacials Working Group: Interglacials of the last 800,000 years, Rev. Geophys., 54, 162–219, https://doi.org/10.1002/2015rg000482, 2016.

Paul, A., Reijmer, J. J. G., Fürstenau, J., Kinkel, H., and Betzler, C.: Relationship between Late Pleistocene sea-level variations, carbonate platform morphology and aragonite production (Maldives, Indian Ocean), Sedimentology, 59, 1640–1658, https://doi.org/10.1111/j.1365-3091.2011.01319.x, 2012.

Petrick, B., Martínez-García, A., Auer, G., Reuning, L., Auderset, A., Deik, H., Takayanagi, H., De Vleeschouwer, D., Iryu, Y., and Haug, G. H.: Glacial Indonesian Throughflow weakening across the Mid-Pleistocene Climatic Transition, Sci. Rep.-UK, 9, 16995, https://doi.org/10.1038/s41598-019-53382-0, 2019.

Prokopenko, A. A., Williams, D. F., Kuzmin, M. I., Karabanov, E. B., Khursevich, G. K., and Peck, J. A.: Muted climate variations in continental Siberia during the mid-Pleistocene epoch, Nature, 418, 65–68, 2002.

Purdy, E. G. and Bertram, G. T.: Carbonate concepts from the Maldives, Indian Ocean, American Association of Petroleum Geologists, https://doi.org/10.1306/St34568, 1993.

Purkis, S., Cavalcante, G., Rohtla, L., Oehlert, A. M., Harris, P., and Swart, P. K.: Hydrodynamic control of whitings on Great Bahama Bank, Geology, 45, 939–942, https://doi.org/10.1130/G39369.1, 2017.

Radice, V. Z., Hoegh-Guldberg, O., Fry, B., Fox, M. D., and Dove, S. G.: Upwelling as the major source of nitrogen for shallow and deep reef-building corals across an oceanic atoll system, Funct. Ecol., 33, 1120–1134, https://doi.org/10.1111/1365-2435.13314, 2019.

Raymo, M. E.: The Initiation of Northern Hemisphere Glaciation, Annu. Rev. Earth Pl. Sc., 22, 353–383, https://doi.org/10.1146/annurev.ea.22.050194.002033, 1994.

Raymo, M. E. and Mitrovica, J. X.: Collapse of polar ice sheets during the stage 11 interglacial, Nature, 483, 453–456, 2012.

Raymo, M. E., Lisiecki, L. E., and Nisancioglu, K. H.: Plio-Pleistocene Ice Volume, Antarctic Climate, and the Global d18O Record, Science, 313, 492–495, https://doi.org/10.1126/science.1123296, 2006.

Reichart, G.-J.: Late Quaternary variability of the Arabian Sea monsoon and oxygen minimum zone, PhD Thesis, Utrecht University, https://dspace.library.uu.nl/handle/1874/31505 (last access: March 2024), 1997.

Reolid, J. and Betzler, C.: The ichnology of carbonate drifts, Sedimentology, 66, 1427–1448, https://doi.org/10.1111/sed.12563, 2019.

Reolid, J., Betzler, C., and Lüdmann, T.: Facies and sedimentology of a carbonate delta drift (Miocene, Maldives), Sedimentology, 66, 1243–1265, https://doi.org/10.1111/sed.12575, 2019.

Reolid, J., Betzler, C., Braga, J. C., Lüdmann, T., Ling, A., and Eberli, G. P.: Facies and geometry of drowning steps in a Miocene carbonate platform (Maldives), Palaeogeogr. Palaeocl., 538, 109455, https://doi.org/10.1016/j.palaeo.2019.109455, 2020.

Rickaby, R. E. M., Bard, E., Sonzogni, C., Rostek, F., Beaufort, L., Barker, S., Rees, G., and Schrag, D. P.: Coccolith chemistry reveals secular variations in the global ocean carbon cycle?, Earth Planet. Sc. Lett., 253, 83–95, 2007.

Rodrigues, T., Alonso-García, M., Hodell, D. A., Rufino, M., Naughton, F., Grimalt, J. O., Voelker, A. H. L., and Abrantes, F.: A 1-Ma record of sea surface temperature and extreme cooling events in the North Atlantic: A perspective from the Iberian Margin, Quaternary Sci. Rev., 172, 118–130, https://doi.org/10.1016/j.quascirev.2017.07.004, 2017.

Rohling, E. J., Grant, K., Bolshaw, M., Roberts, A. P., Siddall, M., Hemleben, C., and Kucera, M.: Antarctic temperature and global sea level closely coupled over the past five glacial cycles, Nat. Geosci., 2, 500–504, 2009.

Saavedra-Pellitero, M., Baumann, K.-H., Ullermann, J., and Lamy, F.: Marine Isotope Stage 11 in the Pacific sector of the Southern Ocean; a coccolithophore perspective, Quaternary Sci. Rev., 158, 1–14, https://doi.org/10.1016/j.quascirev.2016.12.020, 2017.

Saji, N. H., Goswami, B. N., Vinayachandran, P. N., and Yamagata, T.: A dipole mode in the tropical Indian Ocean, Nature, 401, 360, https://doi.org/10.1038/43854, 1999.

Sánchez Goñi, M. F., Ferretti, P., Polanco-Martínez, J. M., Rodrigues, T., Alonso-García, M., Rodríguez-Tovar, F. J., Dorador, J., and Desprat, S.: Pronounced northward shift of the westerlies during MIS 17 leading to the strong 100-kyr ice age cycles, Earth Planet. Sc. Lett., 511, 117–129, https://doi.org/10.1016/j.epsl.2019.01.032, 2019.

Scherer, R. P., Bohaty, S. M., Dunbar, R. B., Esper, O., Flores, J.-A., Gersonde, R., Harwood, D. M., Roberts, A. P., and Taviani, M.: Antarctic records of precession-paced insolation-driven warming during early Pleistocene Marine Isotope Stage 31, Geophys. Res. Lett., 35, L03505, https://doi.org/10.1029/2007GL032254, 2008.

Schlager, W.: Benthic carbonate factories of the Phanerozoic, Int. J. Earth Sci., 92, 445–464, https://doi.org/10.1007/s00531-003-0327-x, 2003.

Schlager, W., Reijmer, J. J. G., and Droxler, A.: Highstand shedding of carbonate platforms, J. Sediment. Res., 64, 270–281, https://doi.org/10.1306/D4267FAA-2B26-11D7-8648000102C1865D, 1994.

Schlanger, S. O.: Strontium Storage and Release During Deposition and Diagenesis of Marine Carbonates Related to Sea-Level Variations, in: Physical and Chemical Weathering in Geochemical Cycles, edited by: Lerman, A. and Meybeck, M., Springer Netherlands, Dordrecht, 323–339, https://doi.org/10.1007/978-94-009-3071-1_15, 1988.

Schulte, S., Rostek, F., Bard, E., Rullkötter, J., and Marchal, O.: Variations of oxygen-minimum and primary productivity recorded in sediments of the Arabian Sea, Earth Planet. Sc. Lett., 173, 205–221, https://doi.org/10.1016/S0012-821X(99)00232-0, 1999.

Shi, F., Yin, Q., Nikolova, I., Berger, A., Ramstein, G., and Guo, Z.: Impacts of extremely asymmetrical polar ice sheets on the East Asian summer monsoon during the MIS-13 interglacial, Quaternary Sci. Rev., 230, 106164, https://doi.org/10.1016/j.quascirev.2020.106164, 2020.

Spratt, R. M. and Lisiecki, L. E.: A Late Pleistocene sea level stack, Clim. Past, 12, 1079–1092, https://doi.org/10.5194/cp-12-1079-2016, 2016.

Sreevidya, E., Sijinkumar, A. V., and Nath, B. N.: Aragonite pteropod abundance and preservation records from the Maldives, equatorial Indian Ocean: Inferences on past oceanic carbonate saturation and dissolution events, Palaeogeogr. Palaeocl., 534, 109313, https://doi.org/10.1016/j.palaeo.2019.109313, 2019.

Stainbank, S., Spezzaferri, S., De Boever, E., Bouvier, A.-S., Chilcott, C., de Leau, E. S., Foubert, A., Kunkelova, T., Pichevin, L., Raddatz, J., Rüggeberg, A., Wright, J. D., Yu, S. M., Zhang, M., and Kroon, D.: Assessing the impact of diagenesis on foraminiferal geochemistry from a low latitude, shallow-water drift deposit, Earth Planet. Sc. Lett., 545, 116390, https://doi.org/10.1016/j.epsl.2020.116390, 2020.

Stoll, H. M. and Schrag, D. P.: Effects of Quaternary sea level cycles on strontium in seawater, Geochim. Cosmochim. Ac., 62, 1107–1118, 1998.

Sun, Y., Clemens, S. C., An, Z., and Yu, Z.: Astronomical timescale and palaeoclimatic implication of stacked 3.6-Myr monsoon records from the Chinese Loess Plateau, Quaternary Sci. Rev., 25, 33–48, 2006.

Sun, Y., Wang, T., Yin, Q., Lyu, A., Crucifix, M., Cai, Y., Ai, L., Clemens, S., and An, Z.: A review of orbital-scale monsoon variability and dynamics in East Asia during the Quaternary, Quaternary Sci. Rev., 288, 107593, https://doi.org/10.1016/j.quascirev.2022.107593, 2022.

Swart, P. K., Oehlert, A. M., Mackenzie, G. J., Eberli, G. P., and Reijmer, J. J. G.: The fertilization of the Bahamas by Saharan dust: A trigger for carbonate precipitation?, Geology, 42, 671–674, https://doi.org/10.1130/g35744.1, 2014.

Tjallingii, R., Röhl, U., Kölling, M., and Bickert, T.: Influence of the water content on X-ray fluorescence core-scanning measurements in soft marine sediments, Geochem. Geophy. Geosy., 8, Q02004, https://doi.org/10.1029/2006GC001393, 2007.

Tomczak, M. and Godfrey, J. S.: Regional Oceanography: An Introduction, Daya Books, ISBN 8170353076, 2003.

Tzedakis, P. C., Hodell, D. A., Nehrbass-Ahles, C., Mitsui, T., and Wolff, E. W.: Marine Isotope Stage 11c: An unusual interglacial, Quaternary Sci. Rev., 284, 107493, https://doi.org/10.1016/j.quascirev.2022.107493, 2022.

Wang, N., Tian, Y., Cao, X., and Wei, M.: Palynological data confirm the occurrence of forest on the Loess Plateau of central China during the Middle Quaternary (MIS13), Palaeogeogr. Palaeocl., 613, 111410, https://doi.org/10.1016/j.palaeo.2023.111410, 2023.

Wang, P.: Global monsoon in a geological perspective, Chinese Sci. Bull., 54, 1113–1136, https://doi.org/10.1007/s11434-009-0169-4, 2009.

Wang, P., Tian, J., Cheng, X., Liu, C., and Xu, J.: Carbon reservoir changes preceded major ice-sheet expansion at the mid-Brunhes event, Geology, 31, 239–242, https://doi.org/10.1130/0091-7613(2003)031<0239:crcpmi>2.0.co;2, 2003.

Wang, P., Li, Q., Tian, J., Jian, Z., Liu, C., Li, L., and Ma, W.: Long-term cycles in the carbon reservoir of the Quaternary ocean: a perspective from the South China Sea, Natl. Sci. Rev., 1, 119–143, https://doi.org/10.1093/nsr/nwt028, 2014.

Webster, P. J.: The Elementary Hadley Circulation, in: The Hadley Circulation: Present, Past and Future, Advances in Global Change Research, vol. 21, edited by: Diaz, H. F. and Bradley, R. S., Springer, Dordrecht, 9–60, https://doi.org/10.1007/978-1-4020-2944-8_2, 2004.

Webster, P. J., Moore, A. M., Loschnigg, J. P., and Leben, R. R.: Coupled ocean–atmosphere dynamics in the Indian Ocean during 1997–98, Nature, 401, 356–360, https://doi.org/10.1038/43848, 1999.

Weirauch, D., Billups, K., and Martin, P.: Evolution of millennial-scale climate variability during the mid-Pleistocene, Paleoceanography, 23, PA3216, https://doi.org/10.1029/2007pa001584, 2008.

Wilson, D. J., Bertram, R. A., Needham, E. F., van de Flierdt, T., Welsh, K. J., McKay, R. M., Mazumder, A., Riesselman, C. R., Jimenez-Espejo, F. J., and Escutia, C.: Ice loss from the East Antarctic Ice Sheet during late Pleistocene interglacials, Nature, 561, 383–386, https://doi.org/10.1038/s41586-018-0501-8, 2018.

Wright, A. K. and Flower, B. P.: Surface and deep ocean circulation in the subpolar North Atlantic during the mid-Pleistocene revolution, Paleoceanography, 17, 1068, https://doi.org/10.1029/2002PA000782, 2002.

Wyrtki, K.: An Equatorial Jet in the Indian Ocean, Science, 181, 262–264, https://doi.org/10.1126/science.181.4096.262, 1973.

Yao, Z., Shi, X., Guo, Z., Li, X., Nath, B. N., Betzler, C., Zhang, H., Lindhorst, S., and Miriyala, P.: Weakening of the South Asian summer monsoon linked to interhemispheric ice-sheet growth since 12 Ma, Nat. Commun., 14, 829, https://doi.org/10.1038/s41467-023-36537-6, 2023.

Yin, Q. Z., Berger, A., and Crucifix, M.: Individual and combined effects of ice sheets and precession on MIS-13 climate, Clim. Past, 5, 229–243, https://doi.org/10.5194/cp-5-229-2009, 2009.

Zeigler, K. E., Schwartz, J. P., Droxler, A. W., Shearer, M. C., and Peterson, L.: Caribbean Carbonate Crash in Pedro Channel at Subthermoclinal Depth During Marine Isotope Stage 11: a Case of Basin-To-Shelf Carbonate Fractionation?, in: Earth's Climate and Orbital Eccentricity: The Marine Isotope Stage 11 Question, American Gephysical Union, 181–204, https://doi.org/10.1029/137GM13, 2003.

Zhisheng, A., Clemens, S. C., Shen, J., Qiang, X., Jin, Z., Sun, Y., Prell, W. L., Luo, J., Wang, S., Xu, H., Cai, Y., Zhou, W., Liu, X., Liu, W., Shi, Z., Yan, L., Xiao, X., Chang, H., Wu, F., Ai, L., and Lu, F.: Glacial-Interglacial Indian Summer Monsoon Dynamics, Science, 333, 719–723, https://doi.org/10.1126/science.1203752, 2011.

Zhisheng, A., Guoxiong, W., Jianping, L., Youbin, S., Yimin, L., Weijian, Z., Yanjun, C., Anmin, D., Li, L., Jiangyu, M., Hai, C., Zhengguo, S., Liangcheng, T., Hong, Y., Hong, A., Hong, C., and Juan, F.: Global Monsoon Dynamics and Climate Change, Annu.

Rev. Earth Pl. Sc., 43, 29–77, https://doi.org/10.1146/annurev-earth-060313-054623, 2015.

Ziegler, M., Jilbert, T., de Lange, G. J., Lourens, L. J., and Reichart, G.-J.: Bromine counts from XRF scanning as an estimate of the marine organic carbon content of sediment cores, Geochem. Geophy. Geosy., 9, Q05009, https://doi.org/10.1029/2007gc001932, 2008.

Ziegler, M., Lourens, L. J., Tuenter, E., and Reichart, G.-J.: High Arabian Sea productivity conditions during MIS 13 – odd monsoon event or intensified overturning circulation at the end of the Mid-Pleistocene transition?, Clim. Past, 6, 63–76, https://doi.org/10.5194/cp-6-63-2010, 2010.